

1 **How have daily climate extremes changed in the recent past over**
2 **northeastern Argentina?**

3 Miguel A. Lovino^{a,1}, Omar V. Müller^a, Ernesto H. Berbery^b, Gabriela V. Müller^a

4 ^a Consejo Nacional de Investigaciones Científicas y Técnicas (CONICET),
5 Centro de Variabilidad y Cambio Climático (CEVARCAM), Facultad de Ingeniería y Ciencias
6 Hídricas, Universidad Nacional del Litoral, Ciudad Universitaria. Ruta Nacional N° 168 - Km 472,4.
7 (3000) Santa Fe, Argentina

8 ^b Earth System Science Interdisciplinary Center/
9 Cooperative Institute for Climate and Satellites-Maryland
10 University of Maryland, College Park, College Park, MD 20742

11 Submitted to Global and Planetary Change: 26 May 2017

12 Revised: 20 February 2018 and 14 June 2018

¹ *Corresponding author address:* Miguel A. Lovino, CONICET, CEVARCAM, FICH, UNL, Ruta Nacional N° 168 – Km 472.4, CC 217, Ciudad Universitaria, 3000 Santa Fe, Argentina. Tel.: +54 342 457 5233x176. E-mail: mlovino@unl.edu.ar.

13

Abstract

14 Changes in climate extremes affect socioeconomics and natural systems in northeastern
15 Argentina (NEA) and may increase its vulnerability leading to unprecedented disasters. This study
16 investigates the long-term changes and interannual variability of daily temperature and precipitation
17 climate extremes and assesses to what extent global reanalyses reproduce the observed variability in
18 the recent past. Datasets include quality-controlled observations (1963-2013) and ERA-Interim and
19 NCEP2 reanalyses (1979-2011). Climate extremes are characterized spatially and temporally by 15
20 indices proposed by the Expert Team on Climate Change Detection and Indices. The leading modes of
21 the area-averaged index time series were obtained by means of a Singular Spectrum Analysis, while the
22 spatial distribution of mean changes was estimated by fitting nonparametric linear trends to each index
23 time series.

24 The results show that temperature extremes are changing toward warmer conditions. The
25 number of warm days has been increasing since 1990 while the number of cold days has been
26 decreasing. Warm and cold nights show a significant signal of warming that seems to be stabilizing in
27 recent decades. Heat waves almost double the frequency and duration of cold waves, and the duration
28 of heat waves increased while cold spells decreased in last decades. Longer heat waves are related to
29 longer dry spells. On the other hand, the number of frost days remained stable although they exhibit
30 high interannual and decadal variability. As well, intense precipitation events in most of the region
31 increased steadily since 1970. The annual maximum amount of 1-day and 5-day precipitation events
32 increased from the 1970s to the 2000s, stabilizing in recent years.

33 The ERA-Interim and NCEP2 reanalyses represent climate extremes with different success. ERA-
34 Interim can recognize temperature extremes in time and space, while the older NCEP2 presents
35 systematic positive errors and has some difficulty to replicate the interannual variability of the number
36 of summer days. Both reanalyses reproduce dry spells and the annual maximum 5-day precipitation
37 with large biases, which are particularly noticeable at each observation station. Although reanalyses

38 would be expected to add information for climate extremes in areas of scarce observations like
39 northeastern Argentina, they still need to be used with great caution and only as a complement to
40 observations, especially in studies focusing on precipitation extremes.

41 **Keywords:** climate extremes; intense precipitation; wet/dry spells; frost days; heat waves; reanalyses.

42 **Highlights:**

- 43 • Since the 1990s, warm days are increasing while cold days are decreasing.
- 44 • The duration of heat waves has increased and cold spells have decreased in last decades.
- 45 • Intense precipitation increased steadily since the 1970s.
- 46 • ERA-Interim reanalysis can describe broad features of area-averaged temperature extremes.
- 47 • ERA-Interim and NCEP2 reanalyses have difficulty in reproducing precipitation extremes.

48 **1. Introduction**

49 Extreme weather and climate events affect ecosystems, disrupt food production and water
50 supply, and negatively impact human settlements causing morbidity and mortality (Field et al., 2014).
51 Increases in extreme events, including their frequency, intensity, spatial extent, and duration may
52 further affect the vulnerability and exposure of ecosystems and human systems. Evidence suggests that
53 temperature extremes have changed toward warmer conditions over most land areas of the world
54 during the past 60 years (Seneviratne et al., 2012; Donat et al., 2013). The number of warm days and
55 warm nights has increased, the number of cold days and cold nights has decreased, and either the
56 length or number of heat waves has increased at the global scale (Seneviratne et al., 2012 and
57 references therein). Although not as statistically significant as for temperature, the number of heavy
58 precipitation events over land areas has increased (Alexander et al., 2006; Seneviratne et al., 2012) and
59 are far more common than regions where the number has decreased (Donat et al., 2013). The changes
60 in extreme events may impact negatively the sustainability of economic development and living
61 conditions requiring the development of coping mechanisms to manage the associated risks (CCSP,
62 2008). Thus, the success in designing coping strategies depends on our understanding of the low
63 frequency climate changes affecting extremes (Klein Tank, 2009).

64 In South America during the last decade (2007-2016), extreme weather and climate events have
65 led to about 7,000 fatalities, more than 58 million people affected, and estimated losses of US\$ 24
66 billion (Guha-Sapir et al., 2015). Frequent and intense precipitation extremes have favored recurrent
67 floods in urban and rural areas (Magrin et al., 2014). According to the IPCC (2012) and Stocker et al.
68 (2013), extreme climate events in this continent have increased in the last decades as reflected in
69 changes in daily extremes of precipitation and temperature (e.g., Haylock et al., 2006; Rusticucci, 2012
70 and Skansi et al., 2013 and references therein). Towards the northern part of the South American
71 continent not enough evidence was found to assume that changes are part of a trend (Seneviratne et
72 al., 2012). However, towards southeastern South America a moderate confidence of a warming in

73 temperature extremes and an increase of intense precipitation events has been detected (e.g.,
74 Fernández-Long et al., 2013; Cavalcanti et al., 2015; Carril et al., 2016 and references therein). Also
75 consistent with global trends, the number of cold nights has decreased and warm nights has increased,
76 the number of warm days has increased and cold days have become fewer (Rusticucci et al., 2016).

77 Northeastern Argentina has great economic and demographic significance as it concentrates
78 most of the agricultural production and the population of the country. Agricultural activities are of key
79 importance for the region's food security, helping to drive its economy, and being a main source of
80 livelihood for the rural population (ECLAC, 2015). Hence, climate extremes affecting agriculture
81 activities can play a significant role in the rise and fall of poverty rates. The region is particularly
82 vulnerable to climate extremes due to its high population density and important economic activities.
83 During the last 10 years, Argentina experienced about 16 floods or landslides with more than 100
84 deaths (Guha-Sapir et al., 2015). Heat waves and cold spells have increased urban mortality rates
85 (Hardoy and Pandiella, 2009), and have affected seasonal crops by decreasing their yields (Verón et al.,
86 2015). There is high statistical confidence that changes in climate extremes are affecting human health
87 by increasing morbidity, mortality, and disabilities, and through the emergence of diseases in previously
88 non-endemic regions (e.g., Winchester and Szalachman, 2009; Carbajo et al., 2012). Further research is
89 expected to provide relevant information that can assist in the elaboration of policies related to
90 adaptation and mitigation of the effects of climate extremes.

91 This study has two main objectives: first, to investigate the long-term changes and interannual
92 variability of daily temperature and precipitation extremes, and second, under the assumption that
93 reanalysis products should add valuable information in regions of scarce observations, to assess to what
94 extent they reproduce the observed variability in the recent past over northeastern Argentina. The
95 structure of the article follows: section 2 introduces the regional context. Section 3 presents the
96 datasets used and the methodological approach. Section 4 examines temperature-related extremes

97 while section 5 analyzes precipitation-related extremes. Section 6 presents a discussion and section 7
98 summarizes the concluding remarks.

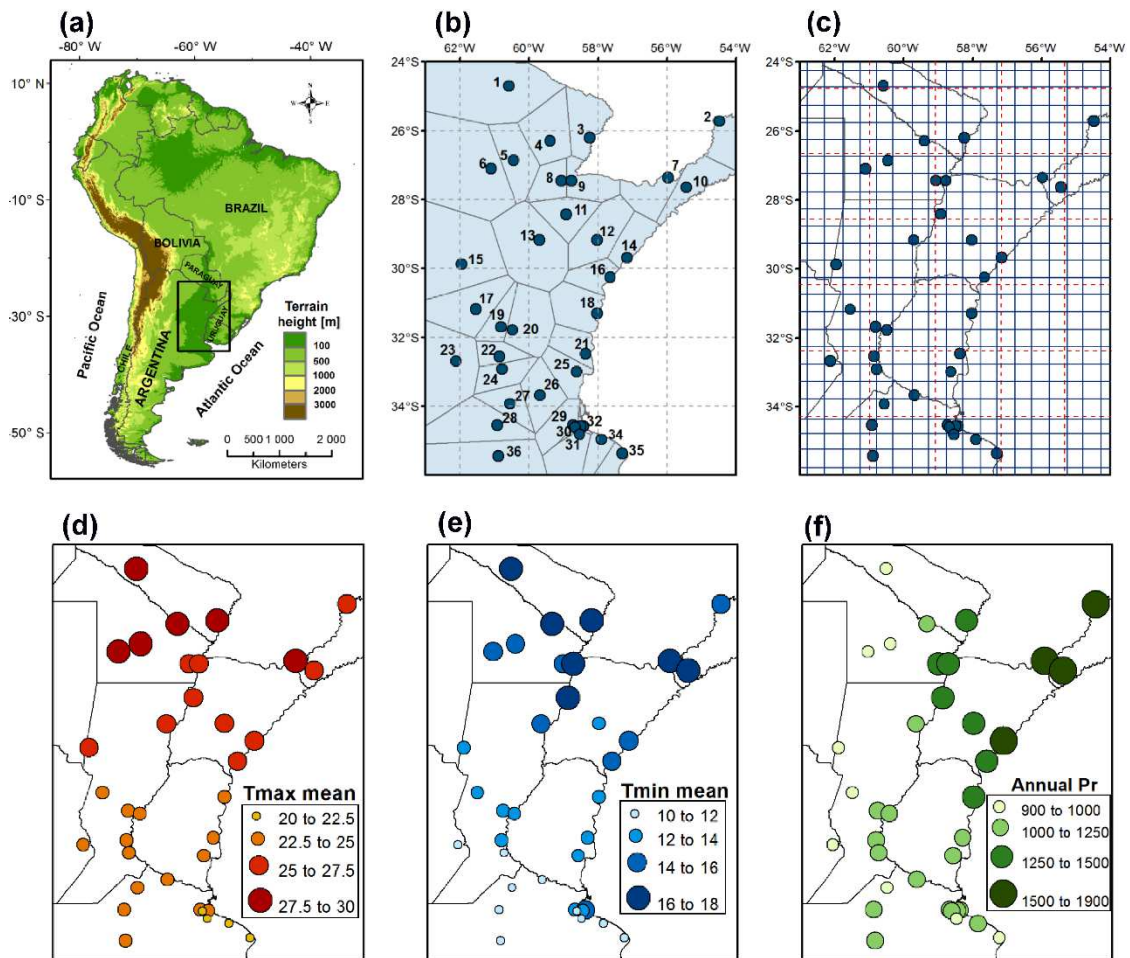
99 **2. Regional Context**

100 This research focuses on northeastern Argentina (NEA), a region that covers the fertile soils of
101 the Pampas and Chaco plains (Fig. 1a). These plains extend for 1,200,000 km² with a mostly flat relief
102 and a slight slope from the northwest to the southeast (NGI, 2015). Regional topographic features favor
103 a markedly latitudinal thermal gradient (Figs. 1d and 1e), with the higher temperatures towards the
104 north (the equatorial side in the SH) and decreasing towards the south. Annual average maximum
105 temperature ranges from 20 °C toward the south to 30 °C toward the north while annual average
106 minimum temperature presents a less pronounced thermal gradient (10 °C to 18 °C).

107 Precipitation towards the northern sector of the domain north of about 20° S (Fig. 1f) is driven
108 by the South American Monsoon System, a fundamental climate feature that controls the austral
109 summer circulation over South America (Zhou and Lau, 1998; Nogués-Paegle et al., 2002; Marengo et
110 al., 2012; Carvallo and Cavalcanti, 2016). The wet season is characterized by an anticyclone located
111 approximately over the Bolivian Altiplano (Lenters and Cook, 1997), and by the Chaco thermal low,
112 centered over northern Argentina (Nogués-Paegle et al., 2002; Marengo et al., 2012). At a more
113 continental scale, the system extends over the ocean in what is known as the South Atlantic
114 Convergence Zone (SACZ) (Kodama, 1992). The South American Low-Level Jet east of the Andes (SALLJ;
115 Virji 1981; Berbery and Collini, 2000) is a key feature of the circulation that remarkably is present
116 throughout the year (Berbery and Barros, 2002). The SALLJ that extends from the southwestern
117 Amazon to southeastern South America is recognized as a key factor that activates convection and
118 precipitation in the subtropical plains of South America (Nogués-Paegle et al., 2002).

119 Mesoscale Convective Systems (MCSs) over Northeastern Argentina during the warm season
120 (October-April) are frequent and account for a large percentage of the total precipitation (Laing and
121 Fritch, 2000). During the austral cold season (May-September), the most important contribution in this
122 region is related to activity at synoptic scale of mean latitudes (Vera et al., 2002). The conjunction of all
123 these climate-forcing factors results in precipitation being distributed during the course of the year
124 (Berbery and Barros, 2002). The resulting spatial pattern of the annual mean precipitation depicts a
125 west-east gradient ranging from 900 mm/year towards the west to more than 1500 mm/year towards
126 the northeast, as shown in Fig. 1f.

127 According to the literature, the variability of the southeastern South America climate at
128 interannual to multidecadal time scales results from the superposition of several large-scale
129 phenomena. El Niño Southern Oscillation (ENSO) is the major source of interannual variability: El Niño
130 conditions might favor wet anomalies, intensify warm spells and reduce frost days while La Niña
131 conditions might favor dry anomalies and increased cold events (Müller et al., 2000; Grimm and
132 Tedeschi, 2009; Rusticucci et al., 2016). The Southern Annular Mode, and the South Atlantic and Pacific
133 Oceans also modulate the interannual variability of extreme temperature frequencies (Barrucand et al.,
134 2008; Loikith et al., 2017). Pacific decadal variability (PDV), the Atlantic Ocean and the SACZ are the
135 main climate forcing factors of the southeastern South America climate variability on interannual to
136 multidecadal time scales (Kayano and Andreoli, 2007; Mo and Berbery, 2011; Barreiro et al., 2014;
137 Grimm et al., 2016).



138 **Fig. 1. (a)** Topography map of South America and the main countries of southern South America.
 139 The study region in northeastern Argentina is highlighted with a black rectangle. **(b)** Spatial
 140 distribution of stations with long records of high-quality datasets of observed precipitation and
 141 temperature (description in Table 1) and the Thiessen polygons used to compute the areal-
 142 average of the variables. **(c)** Grid resolution of the reanalyses: ERA-Interim (blue full lines) and
 143 NCEP2 (red dashed lines). Climatological mean values (1963-2013 period) of the **(d)** annual
 144 average maximum temperature, **(e)** annual average minimum temperature and, **(f)** annual
 145 precipitation.

146 **3. Methodology**

147 **3.1 Datasets**

148 In-situ observations of daily precipitation as well as daily maximum and minimum temperatures
149 for 1963-2013 were used for the present study. They were provided by the Argentine National Weather
150 Service and the Argentine National Institute of Agricultural Technology. About 36 stations were selected
151 for the quality and extent of the records (see Fig. 1b and other details in Table 1). To be included,
152 stations were required to exceed a threshold of 90% of days with data availability. As shown in Table 1,
153 most of the selected stations (29 out of 36) had more than 95% of days with data. Missing values were
154 filled using the normal ratio method to interpolate from nearby stations (Young et al., 1992). A linear
155 regression approach was applied in exceptional cases when there was only one neighboring station
156 with data in the period to be filled. Neighboring stations were selected according to their maximum
157 correlation with the station to be completed. Finally, a quality control of the completed time series was
158 carried out to identify non-systematic errors, ensure the absence of outliers and the internal
159 consistency of the records (the latter assessed with the RHtestsV3 method developed by Wang et al.,
160 2010).

161 The ERA-Interim (Dee et al., 2011) and the NCEP-DOE Reanalysis 2 (NCEP2, Kanamitsu et al.,
162 2002) were used for the common period from 1979 to 2011. The ERA-Interim is used on a regular grid
163 at 0.5° spatial resolution, while the NCEP2 spatial resolution is 1.875° latitude x 1.904° longitude (see
164 Fig. 1c). The reanalyses offer a full coverage on areas with scarce gauge stations like the northwest
165 portion of the domain (see Fig. 1b).

Table 1. Meteorological stations used in this study with information in the 1963-2013 period.

	Station	Latitude	Longitude	Missing Data (%)
1	Las Lomitas	-24.70	-60.58	0.83
2	Iguazú airport	-25.73	-54.47	5.96
3	Formosa airport	-26.20	-58.23	0.28
4	El Colorado	-26.3	-59.38	8.97
5	Roque Sáenz Peña	-26.87	-60.45	4.30
6	Las Breñas	-27.10	-61.10	2.35
7	Posadas airport	-27.36	-55.96	3.41
8	Resistencia airport	-27.45	-59.05	6.51
9	Corrientes airport	-27.45	-58.77	5.53
10	Cerro Azul	-27.65	-55.43	3.91
11	Bella Vista	-28.43	-58.92	2.03
12	Mercedes	-29.17	-58.02	6.68
13	Reconquista airport	-29.18	-59.70	1.80
14	Paso de los Libres airport	-29.68	-57.15	2.90
15	Ceres airport	-29.88	-61.95	5.83
16	Monte Caseros airport	-30.26	-57.65	0.33
17	Rafaela	-31.18	-61.55	0.84
18	Concordia airport	-31.30	-58.02	0.18
19	Sauce Viejo airport	-31.70	-60.82	0.50
20	Paraná airport	-31.78	-60.48	0.14
21	Concepción del Uruguay	-32.48	-58.35	4.16
22	Oliveros	-32.55	-60.85	0.47
23	Marcos Juárez	-32.68	-62.12	0.12
24	Rosario airport	-32.92	-60.78	0.78
25	Gualedaychú airport	-33.00	-58.62	0.79
26	San Pedro	-33.68	-59.68	5.40
27	Pergamino	-33.93	-60.55	4.00
28	Junín airport	-34.55	-60.92	0.02
29	San Miguel	-34.55	-58.73	2.54
30	Aeroparque airport	-34.57	-58.42	1.82
31	Buenos Aires	-34.58	-58.48	0.09
32	Castelar	-34.60	-58.67	0.21
33	Ezeiza airport	-34.82	-58.53	3.11
34	La Plata airport	-34.96	-57.90	3.83
35	Punta Indio	-35.37	-57.28	4.15
36	9 de Julio airport	-35.45	-60.88	1.25

167 **3.2 Indices of extreme climate**

168 The more relevant NEA extreme events are those that involve precipitation and temperature.
169 Dry and wet spells, as well as frosts, are most critical for agriculture. Heat waves are also relevant for
170 human wellbeing. To examine these phenomena, we employ a subset of ETCCDI² indices that
171 characterize the intensity, duration and frequency of climate events (Klein Tank et al., 2009 and Zhang
172 et al., 2011). The core set of ETCCDI indices, computed from daily temperature and precipitation, was
173 developed to detect and attribute changes and evaluate long-term variability in climate extremes.
174 ETCCDI indices are statistically robust, can cover a wide range of climates and have a high signal-to-
175 noise ratio. Of the 27 core indices proposed by ETCCDI, we analyze ten that are temperature-based and
176 five based on precipitation as the most relevant for extreme events that have greatest impact in NEA
177 (see Table 2). The indices are categorized as absolute, duration, or threshold indices (Sillman et al.,
178 2013): (i) absolute indices represent the intensity of extreme events, for instance, the annual maximum
179 precipitation amounts per day; (ii) duration indices describe the length in days of wet/dry spells, or
180 warm/cold spells; lastly, (iii) threshold indices count the number of days when a threshold is exceeded,
181 characterizing the frequency of extreme events. Percentile-based threshold indices allow for spatial
182 comparisons because they are independent of the spatial variability and they sample the same part of
183 the probability distribution of a variable at each location (Zhang et al., 2011). In this study, a
184 bootstrapping approach (Zhang et al., 2005) was applied to remove inhomogeneities near the beginning
185 and end of the period in percentile-based indices, avoiding possible biases in the trend estimation.

186 The indices were evaluated in space and time. The most recent normal period of the time
187 series, 1981-2010, was selected as the base period for the calculation of percentile indices and to
188 compute anomalies of the other indices (in agreement with Zhang et al., 2011 and Skansi et al., 2013).
189 We have verified that the choice of a different normal period (e.g. 1971–2000) and even the full data

² World Meteorological Organization (WMO) Commission for Climatology (CCI)/CLIVAR/ JCOMM Expert Team on Climate Change Detection and Indices (ETCCDI)

190 period (1963-2013) has negligible effects on the results with changes in the indices of less than 2%. To
191 depict their spatial distribution, the mean climatology values of the observation-based and reanalysis-
192 based indices were estimated as the average over their corresponding available periods, i.e., 1963-2013
193 and 1979-2011 respectively.

194 Area-averaged time series were computed using the Thiessen Polygons method (Okabe et al.,
195 2000) in each time step to take into account the uneven spatial distribution of the stations (see Fig. 1b).
196 This method calculates station weights based on the relative areas of each measurement station in the
197 Thiessen polygon network (Fig. 1b). The individual weights are multiplied by the station observation
198 index and the values are summed to obtain the areal average index in each time step.

199 **Table 2.** ETCCDI indices used in this study, adapted from Donat et al. (2013) and Sillman et al.
 200 (2013). TX_{ij} and TN_{ij} are the daily maximum and minimum temperature respectively on day i in period j
 201 (where period is year except for DTR that is season). TX_{in90} or TX_{in10} (TN_{in90} or TN_{in10}) are the calendar
 202 day 90th or 10th percentile of daily maximum (minimum) temperature calculated for a 5-day window
 203 centered on each calendar day n from the base period 1981-2010.

Temperature-based Indices				
	Index	Index Name	Index definition	Unit
Frequency	TX90p	Warm days	Percentage of annual days when $TX_{ij} > TX_{in90}$	% of days
	TX10p	Cold days	Percentage of annual days when $TX_{ij} < TX_{in10}$	% of days
	TN90p	Warm nights	Percentage of annual days when $TN_{ij} > TN_{in90}$	% of days
	TN10p	Cold nights	Percentage of annual days when $TN_{ij} < TN_{in10}$	% of days
	SU25	Summer days	Annual number of days when $TX_{ij} > 25$ °C	days
	TR	Tropical nights	Annual number of days when $TN_{ij} > 20$ °C	days
	FD	Frost days	Annual number of days when $TN_{ij} < 0$ °C	days
Intensity	DTR	Diurnal temperature range	Mean difference between daily maximum and daily minimum temperature: If I represents the number of days in j , then $DTR_j = \frac{\sum_{i=1}^I TX_{ij} - TN_{ij}}{I}$	°C
Duration	WSDI	Warm spell duration indicator	Annual number of days with at least 6 consecutive days when $TX_{ij} > TX_{in90}$	days
	CSDI	Cold spell duration indicator	Annual number of days with at least 6 consecutive days when $TN_{ij} < TN_{in10}$	days
Precipitation-based Indices				
Intensity	RX1day	Max 1-day precipitation	Annual maximum 1-day precipitation amount	mm
	RX5day	Max 5-day precipitation	Annual maximum consecutive 5-day precipitation amount	mm
	SDII	Simple daily intensity index	Annual total precipitation divided by the number of wet days (i.e., when precipitation ≥ 1 mm)	mm/day
Duration	CWD	Consecutive wet days	Maximum annual number of consecutive wet days (i.e., when precipitation ≥ 1 mm)	days
	CDD	Consecutive dry days	Maximum annual number of consecutive dry days (i.e., when precipitation < 1 mm)	days

204 **3.3 Trends and variability modes of climate extreme indices**

205 A Singular Spectrum Analysis (Ghil et al., 2001; Wilks, 2006) was employed to obtain the trends
206 and leading modes of the area-averaged time series of each index. We focus on nonlinear trends, which
207 allow assessing the temporal evolution of long-term changes in extreme climate events. The SSA
208 method also detects oscillatory modes that can provide important information of the temporal
209 variability of the climate-related extremes.

210 The SSA method describes the variability of a time series by its eigenvalue decomposition into
211 temporal-empirical orthogonal functions (T-EOFs, eigenvectors) and temporal-principal components (T-
212 PCs). Each T-PC represents a filtered version of the original time series with a portion of the variance
213 associated with its corresponding eigenvalue. A quasi-oscillatory structure can be found when two
214 consecutive eigenvalues are nearly equal and their associated T-PCs are in quadrature. A nonlinear
215 trend is obtained when the estimation error of a leading eigenvalue, here computed following Ghil and
216 Vautard (1991), does not overlap with other eigenvalues and its corresponding T-PC is slowly varying
217 and uncorrelated with other T-PCs (Vautard, 1995; Wilks, 2006). Finally, a significance test against a red
218 noise null-hypothesis using a Monte Carlo method (Allen and Smith, 1996) with an ensemble of 1,000
219 independent realizations was applied to distinguish significant T-PCs at the 95% confidence level.

220 The choice of the window length M in the SSA is crucial since it limits the longer periods that the
221 SSA can resolve. Window length should not exceed one third of the time series length to adequately
222 represent cycles between $M/5$ and M (Vautard, 1995). Considering the length of the data period
223 available ($N = 51$ years), we use a window length $M = 10$ years. Thus, in this study, interannual
224 variability represents the spectrum between 2 and 10 years (following Krepper and García, 2004 and
225 Krepper et al., 2006). With the window length of $M = 10$ years chosen here, the SSA-method cannot
226 identify periods at decadal-to-multidecadal time scales. Our analysis will thus focus on nonlinear trends
227 and frequencies of interannual variability cycles.

228 In cases when the SSA method does not clearly detect nonlinear trends, i.e. when the errors of
229 the eigenvalues overlap preventing the separation of a significant trend signal, a 10-yr moving average,
230 consistent with M=10 years, was used to represent the low frequency variability. Ten-year moving
231 averages filter signals with frequencies higher than 10 years and represent in a simpler way the low
232 frequency behavior of the time series.

233 Changes in extreme climate events at each station were assessed by fitting linear trends to the
234 indices in the 51-year period. The magnitudes of the trends were computed adapting the
235 nonparametric Kendall's tau based slope estimator (Sen, 1968) and using the method originally
236 proposed by Zhang et al. (2000) and later refined by Wang and Swail (2001). Trends of all indices were
237 tested for statistical significance at the 95% confidence level following the approach of Bronaugh and
238 Werner (2013).

239 **3.4 Reanalyses skill evaluation**

240 The skill of ERA-Interim and NCEP2 to reproduce temperature and precipitation extremes is
241 assessed, first, contrasting the spatial and temporal climatology fields against observations, and second,
242 using objective statistical metrics. The metrics used are the Pearson correlation coefficient (r), the mean
243 bias error (MBE), and the root mean square error (RMSE). A definition of these metrics can be found in
244 Déqué (2012).

245 Northeastern Argentina presents an irregular distribution of the observation stations, as noted
246 above (see Fig. 1b). Therefore, comparisons between grid cell products with station observations
247 necessarily involve interpolations, which introduces new errors (Wang and Zeng, 2012). To minimize
248 these interpolation errors, we follow the approach in Wang and Zeng (2012), Jones et al. (2016), Yang
249 and Kim (2017) and Zhang et al. (2017) by comparing data from each station with those from a
250 reanalysis grid cell covering this station. It should be noted that given the lack of topographic

251 characteristics of the region (see Fig. 1a), there are no sharp gradients and the variations of the climatic
252 variables are largely unaffected by their spatial resolution.

253 The ability of the reanalyses to represent temperature extremes is evaluated by means of three
254 fixed-threshold indices: summer days, tropical nights and frost days (SU25, TR and FD respectively; see
255 their definitions in Table 2). These indices were selected for two reasons: first, they avoid the
256 complexity of percentile-based indices, which are difficult to replicate in reanalysis (estimated but not
257 shown; see also Sillman et al., 2013), and second, because they are relevant to the agro-industrial
258 activities in the region. For precipitation extremes, the annual maximum 5-day amounts (RX5day) and
259 the annual maximum consecutive dry days (CDD) are evaluated (see the indices definitions in Table 2).
260 As suggested by Sillman et al. (2013), reanalyses tend to underestimate the magnitude of extreme
261 precipitation events characterized by the annual maximum 1-day amount (RX1day, Table 2), but they
262 may have greater ability to reproduce the CDD and RX5day because dry conditions and 5-day
263 precipitation events are usually of larger spatial scale than daily extreme precipitation events.

264 4. Temperature-related climate extremes

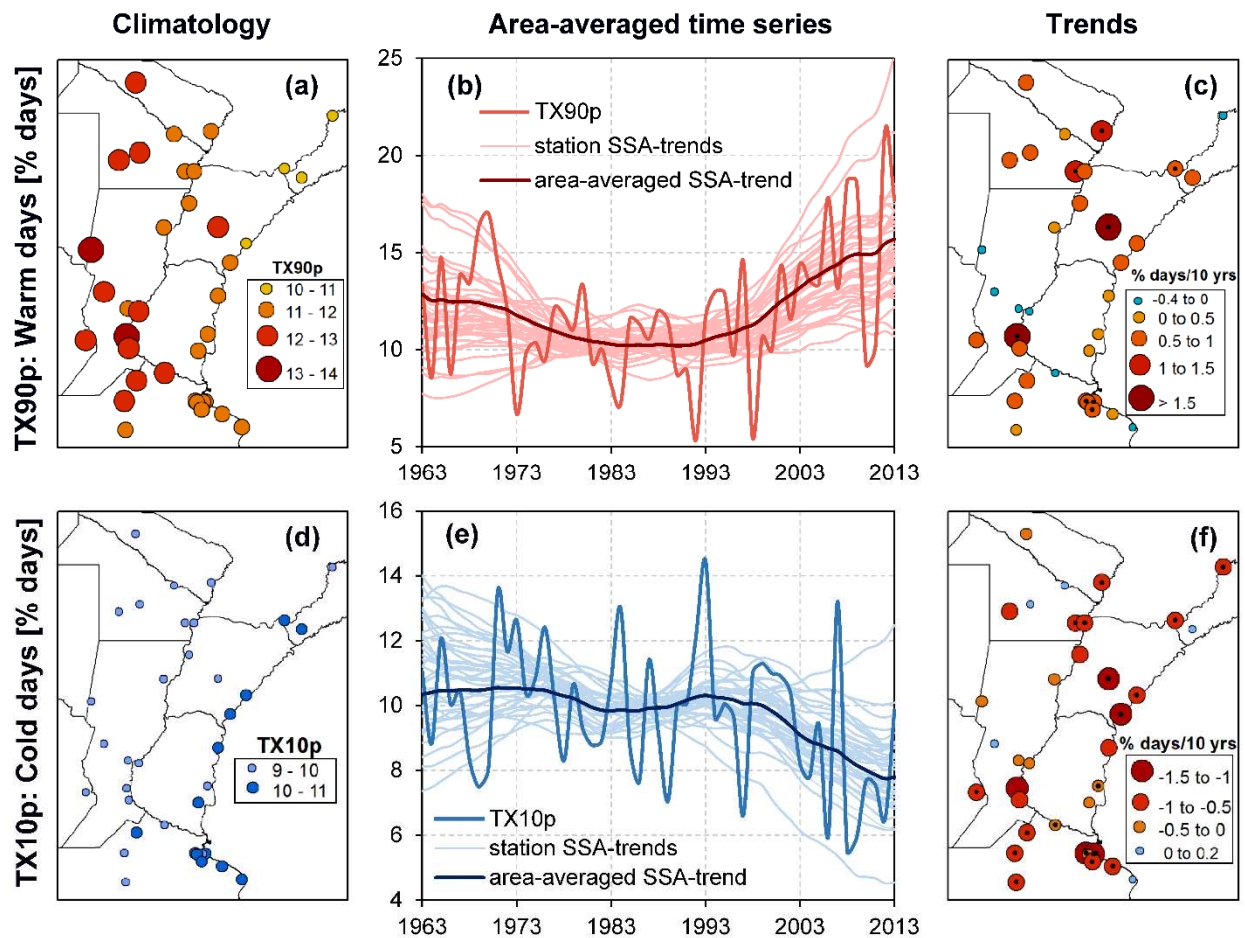
265 4.1 Maximum-temperature frequency extremes

266 The frequency of days per year when the maximum temperature exceeds the 90th percentile
267 (TX90p) will be referred to as warm days. The frequency of days when the maximum temperature is
268 below the 10th percentile (TX10p) will be referred to as cold days. The climatology of warm days (Fig.
269 2a) has an almost longitudinal gradient that ranges from 14% of days per year towards the west to 10%
270 towards the northeast. The warm days are influenced by interannual variability with a periodicity close
271 to 9 years (Table 3) which explains 30% of the variance of the total time series. Fig. 2b (and Table 3) also
272 reveals a nonlinear trend of the frequency of warm days, which had slightly decreased before the
273 1990s, but since then it has experienced a steady increase of about 5%. Despite the dispersion among
274 the trends of TX90p for all stations (thin lines in Fig. 2b), they exhibit a common behavior. The spatial
275 distribution of the trends in Fig. 2c reveals that most stations have increases of warm days, particularly
276 towards the northeast. Only a few stations (7 out of 36) experienced a decrease, and it was non-
277 significant.

278 Days with the maximum temperature in the lowest 10th percentile (cold days), shown in Fig. 2d,
279 are less frequent than warm days and almost uniform for the region, with a slight increase towards the
280 east from 9% to 11% of cold days in a year. The area-averaged frequency of colds days presented in Fig.
281 2e reveals a decrease from 10% to 7.5% of days per year since about 1990 with an important
282 interannual variability. The spatial distribution of the linear trends presented in Fig. 2f shows the largest
283 decrease of cold days towards the east, where cold days are more frequent.

Table 3. Summary of the main variability modes of temperature-related extremes found with SSA.

SSA Results of Temperature-based Indices					
	Index	Index Name	Components	Trend or Dominant Period (year/cycle)	Explained variance (%)
Frequency	TX90p	Warm days	T-PC1	Trend	27
			T-PC2 and T-PC3		8.8
	TX10p	Cold days	T-PC1	Trend	18
	TN90p	Warm nights	T-PC1	Trend	18
			T-PC2 and T-PC3		4
	TN10p	Cold nights	T-PC1	Trend	36
T-PC2 and T-PC3			4	28	
FD	Frost days	T-PC1 and T-PC2		4	42.5
Intensity	DTR summer	Summer diurnal temperature range	T-PC1	Trend	21
	DTR winter	Winter diurnal temperature range	No significant modes		
Duration	WSDI	Warm spell duration indicator	T-PC1	Trend	20
	CSDI	Cold spell duration indicator	T-PC1	Trend	43.5



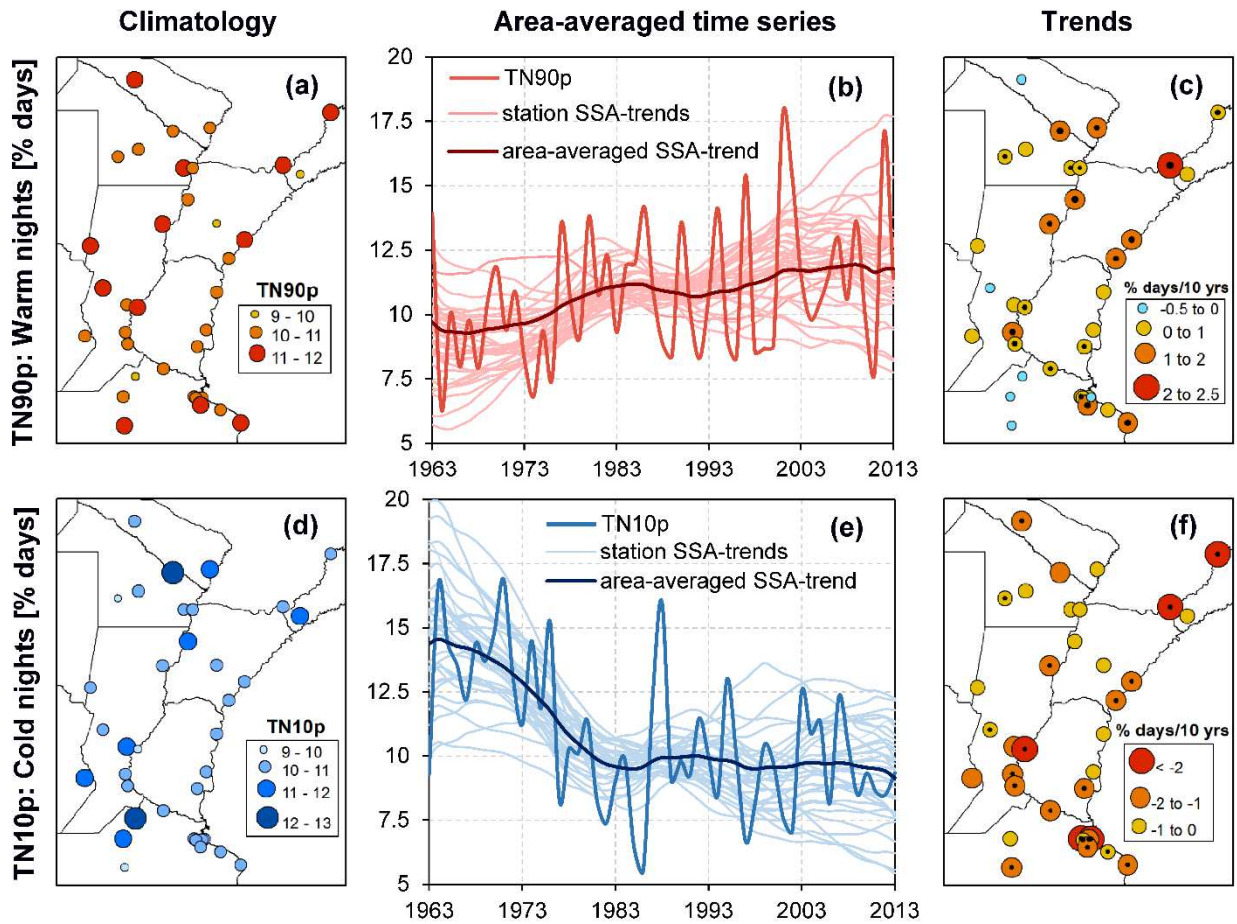
285 **Fig. 2.** Frequency of maximum temperature (daytime) climate extremes characterized by warm days
 286 (TX90p) and colds days (TX10p), defined as the percentage of annual days when $T_{max} > 90^{th}$
 287 percentile and $T_{max} < 10^{th}$ percentile, respectively. Left panels (a, d): climatological mean values in
 288 the 1963-2013 period. Middle panels (b, e): the temporal evolution of the area-averaged indices and
 289 their trends. Right panels (c, f): the spatial distribution of the linear trends. Warm colors (yellow to
 290 red) indicate a shift toward warmer conditions while cold colors (light blue to blue) toward colder
 291 conditions. Stations highlighted with a black dot indicate a significant linear trend, at least at the 95%
 292 confidence level.

293

294 4.2 Minimum-temperature frequency extremes

295 Figure 3 presents the indices characterizing the frequency of minimum-temperature extremes.
296 The indices TN90p and TN10p (Table 2) describe respectively the percentage of nights when minimum
297 temperature was in the 90th percentile (warm nights) and the percentage of nights when it was in the
298 lowest 10th percentile (cold nights). The annual mean climatology of warm nights (Fig. 3a) presents
299 values between 9% and 12% of days without a clear spatial pattern. Fig. 3b indicates that warm nights
300 exhibit an area-averaged positive nonlinear trend, more evident from the late 1960s to the early 1980s.
301 From 1980 to 2013, the trend is also positive but with lower magnitude, being strongly influenced by
302 interannual variability. It is of interest to examine the individual stations trends (thin lines). They exhibit
303 smaller dispersion around the 1980s, with a marked dispersion increase during latter years. Aside from
304 the trends, a 4-yr mode of variability explains almost 30% of the TN10p and TN90p variances (see Table
305 3). Fig. 3c shows that the number of warm nights presents the greatest increases towards the north (1%
306 to 2% of days per decade), with 11 out of 19 stations with significant rising trends. Only a few stations
307 (about 6) had a non-significant negative trend.

308 The frequency of cold nights (Fig. 3d) ranges from 9% to 13% of annual days, again without a
309 well-defined spatial pattern. Their mean trend, presented in Fig. 3e, shows that there was about a 5%
310 decrease in the frequency of cold nights from the 1960s to 1980s, that is, at the same time when an
311 increase of about 3% was observed in the frequency of warm nights (Fig. 3b). According to Fig. 3f, the
312 decrease in cold nights occurred in the whole region, with 21 stations having significant trends at least
313 at the 95% confidence level.



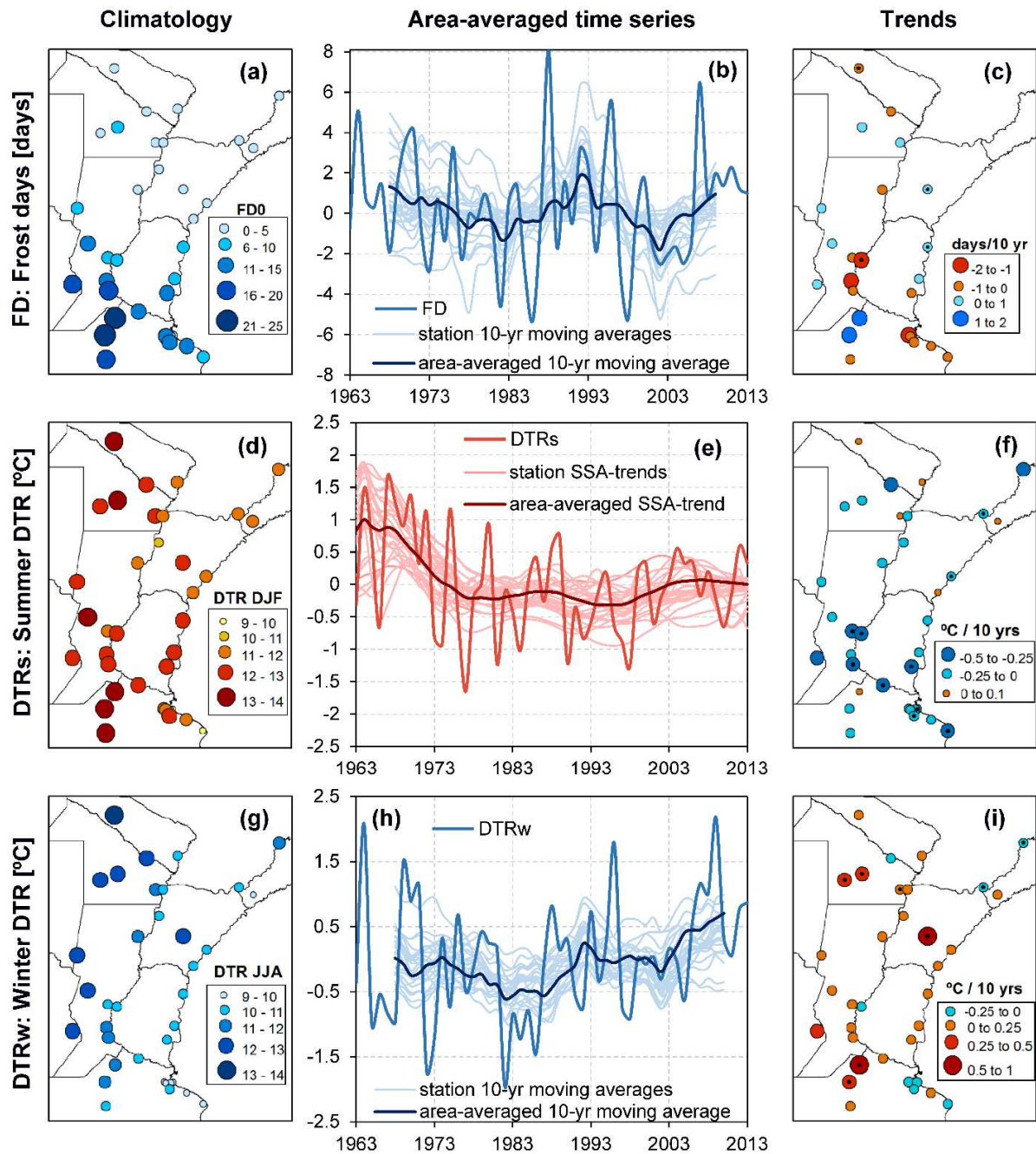
314 **Fig. 3.** Frequency of minimum temperature (nighttime) climate extremes characterized by warm
 315 nights (TN90p) and colds nights (TX10p), defined as the percentage of annual days when $T_{min} > 90^{th}$
 316 percentile and $T_{min} < 10^{th}$ percentile, respectively. Left panels (a, d): climatological mean values in
 317 the 1963-2013 period. Middle panels (b, e): the temporal evolution of the area-averaged indices and
 318 their trends. Right panels (c, f): the spatial distribution of linear trends. Warm colors (yellow to red)
 319 indicate a shift toward warmer conditions while cold colors (light blue to blue) toward colder
 320 conditions. Stations highlighted with a black dot indicate a significant linear trend, at least at the 95%
 321 confidence level.

322 **4.3 Frost events and diurnal temperature range**

323 Many crops are sensitive to the number of frost days (FD) and to the diurnal temperature range
324 (DTR) defined in Table 2. These indicators of temperature-related extremes provide useful information
325 for agricultural planning. Fig. 4 displays the climatology, areal-averaged temporal evolution and spatial
326 distribution of local trends of these indicators. Consistent with the minimum temperature climatology
327 (Fig. 1e), the frequency of frost days varies latitudinally, decreasing from almost 25 days per year
328 towards the south to less than 5 days per year to the north (Fig. 4a). Frost days do not have a noticeable
329 trend (Figs. 4b and 4c), but they do exhibit interannual and decadal variability. On interannual scales, a
330 4-yr mode is consistent with the cycle discussed for minimum-temperature extremes, particularly in
331 cold nights, explaining 42.5% of the FD variance (Table 3).

332 During austral summer, the diurnal temperature range (DTRs) varies between 10 °C and 14 °C
333 with highest values towards the west (Fig. 4d). The nonlinear area-averaged SSA-trend in Fig. 4e
334 indicates that DTRs decreased substantially between the 1960s and 1970s, and remained constant from
335 the 1980s to the present. The local trends shown in Fig. 4f exhibit negative values over most of the
336 region, with largest negative trends of up to 0.5 °C in magnitude per decade towards the south. Almost
337 negligible positive trends (<0.1 °C) are found in very few stations, without any clear pattern.

338 During winter, the diurnal temperature range (DTRw) in Fig. 4g has a similar pattern as in
339 summer, ranging from 14 °C towards the west to 9 °C towards the east. Changes in time of the area-
340 averaged DTRw (Fig. 4h) reveal a decrease in the earlier period and a continued increase from the
341 1990s to the present. Fig. 4i suggests that the entire region experienced an increase in the DTR, with 28
342 out of 36 stations having positive trends.

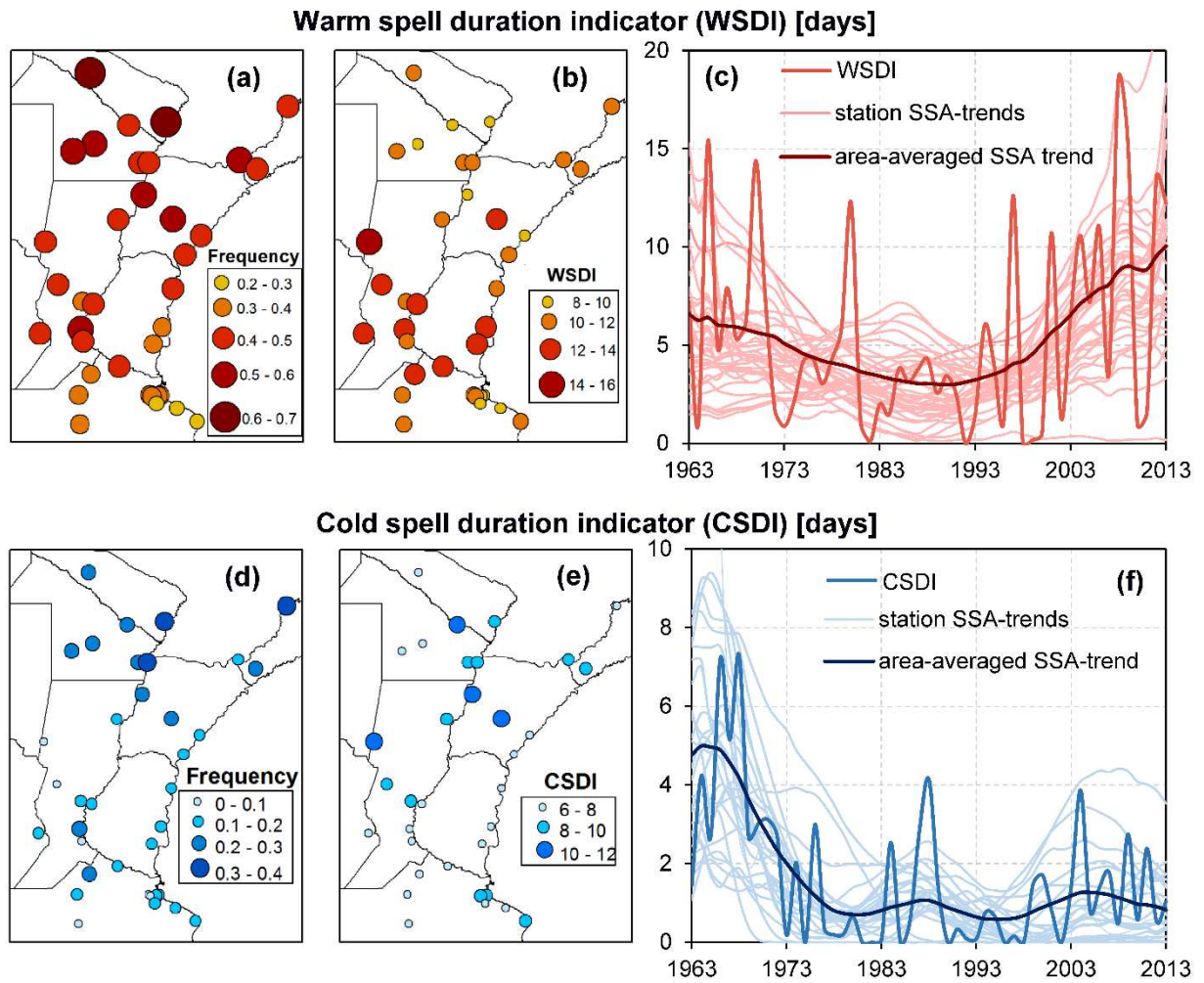


343 **Fig. 4.** Number of frost days (FD, first row) and the diurnal temperature range during summer (DTRs,
 344 second row) and winter (DTRw, third row). Left panels (a, d, g): climatological mean values in the
 345 1963-2013 period. Middle panels (b, e, h): the temporal evolution of the area-averaged indices and
 346 their trends. Right panels (c, f, i): the spatial distribution of linear trends. Warm colors (yellow to red)
 347 indicate a shift toward warmer conditions while cold colors (light blue to blue) toward colder
 348 conditions. Stations highlighted with a black dot indicate a significant linear trend, at least at the 95%
 349 confidence level.

350 **4.4 Duration of warm and cold spells**

351 Agriculture and human settlements may be severely affected by heat and cold waves. The warm
352 spell duration indicator (WSDI) is defined as the annual count of days with at least six continuous days
353 when maximum temperature exceeds the 90th percentile (see Table 2). The index for cold waves follows
354 an equivalent definition, as it corresponds to the annual count of days with at least six continuous days
355 that have a minimum temperature within the 10th percentile. Note that in principle WSDI and CSDI are
356 not necessarily related to latitudinal changes, since they account for the number of days exceeding a
357 percentile-threshold. Yet, some spatial structures can be identified. Figs. 5a-c present the mean annual
358 frequency, duration and area-averaged temporal evolution of warm spells. It can be seen that heat
359 waves are more frequent (Fig. 5a) but of shorter duration (Fig. 5b) towards the north, where there is up
360 to 70% of chance of a heat wave per year with a duration of about 8 to 12 days. Towards the south,
361 heat waves are less frequent but can last longer, up to about 16 days. The evolution of WSDI shown in
362 Fig. 5c indicates that warm spell duration slightly decreased during the first half of the period, and then
363 increased from the 1990s to present. The highest anomaly value of the WSDI was registered in 2008
364 with an average of more than 20 consecutive days, when the whole region experienced a severe
365 drought and heat wave (Müller et al., 2014; Rusticucci et al., 2015). Indeed, some stations in the south-
366 center registered WSDI of more than 60 days.

367 The cold waves (CSDI) are more frequent (Fig. 5d) and of longer duration (Fig. 5e) towards the
368 north, where minimum temperatures are higher than in the south (see Fig. 1e). For example, the
369 probability of having one 10-day cold wave per year is 40% while towards the colder south, the
370 probability of a cold wave is below 20%. The temporal evolution of the area-averaged CSDI (Fig. 5f)
371 indicates that cold spell duration decreased markedly in the mid-1960s and remained at about the same
372 level since then. A strong decadal variability is noticed throughout the period.



373 **Fig. 5.** Metrics of warm and cold spell duration (definitions are given in Table 2). Frequency of at least
 374 one event per year in **(a)** and **(d)**; average duration in years with occurrence in **(b)** and **(e)**; area-
 375 averaged time series in **(c)** and **(f)**.

376 **4.5 Temperature-related extremes in reanalyses**

377 So far we have examined extremes as identified by station observations which do not have a
378 complete coverage of the study region. Global reanalysis offer full data coverage in time and space
379 based on a global model that assimilates diverse kinds of observations. Then, it is of interest to assess
380 whether reanalysis products can be used as a complement to observations in northeastern Argentina
381 where there is a limited coverage of gauge stations. In this sub-section, we examine the skill of two
382 reanalysis (NCEP2 and ERA-Interim) to reproduce maximum-temperature extremes (characterized by
383 summer days) and minimum-temperature extremes (represented by tropical nights and frost days). In
384 addition to the already defined FD index, the summer days index (SU25) is obtained as the annual
385 number of days when $T_{max} > 25$ °C; and the tropical nights index (TR) is computed as the annual
386 number of days when $T_{min} > 20$ °C (see details on Table 2). These two indices have a latitudinal
387 dependence with larger values towards lower latitudes.

388 **4.5.1 Number of summer days (SU25)**

389 The overall characteristics of the SU25 index are presented in Fig. 6a. The spatial field from the
390 reanalysis are superimposed by circles of the corresponding values obtained from observations. A visual
391 inspection suggests that there is similarity between the spatial pattern identified in observations and
392 reanalyses. NCEP2, an older reanalysis product, overestimates the field of observed summer days
393 towards the south. According to Fig. 6a (right panel), the area-averaged SU25 estimated from ERA-
394 Interim follows the temporal evolution of the observations-based SU25 with a mean bias error of only 3
395 days and a correlation coefficient close to 0.9. However, the interannual variability of the area-averaged
396 SU25 is not properly represented by NCEP2, with a correlation coefficient of 0.51.

397 Statistical metrics for SU25 index computed from reanalyses at each station location are presented
398 in Fig. 7. ERA-Interim achieves the best performance, particularly towards the south, with most

399 correlations to observations exceeding 0.7 (see histogram below map in Fig. 7a). In contrast, the older
400 NCEP2 shows lower values with the most frequent correlations in the range between 0.4 and 0.6 (see
401 histogram below map in Fig. 7b).

402 Figures 7c and 7d show that the two reanalyses have mostly positive mean bias errors, with ERA-
403 Interim having an overestimation of up to 10 summer days in most stations. The older NCEP2 shows
404 positive biases in the range of 10-20 days and larger. Consistently, Figs. 7e and 7f indicate that the most
405 frequent RMSE values for ERA-Interim are less than 20 days, while those for NCEP2 exceed 20 days.

406 **4.5.2 Number of tropical nights (TR)**

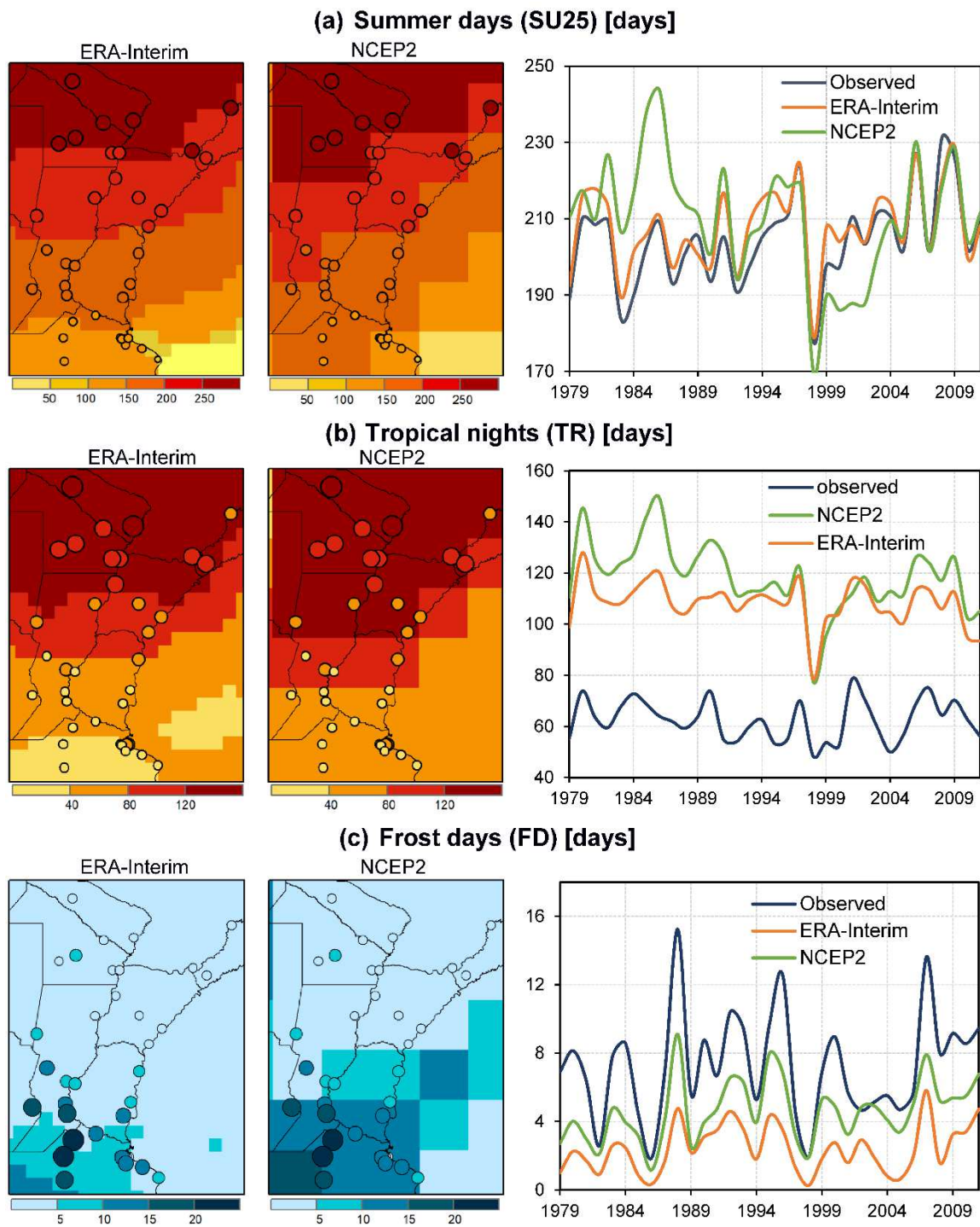
407 The mean fields of the number of tropical nights (days with $T_{min} > 20\text{ }^{\circ}\text{C}$) in Fig. 6b show the
408 expected increase towards the lower latitudes in both observations and reanalysis. The two reanalyses
409 reproduce the south-north gradient but with a larger number of tropical nights towards the south. This
410 overestimation is more noticeable in the area-averaged time series (right panel). The observed mean
411 value of tropical nights is 56 days, while the ERA-Interim and NCEP2 have a larger number, 102 and 112
412 days respectively. The time series shows that both reanalyses retain information about the interannual
413 variability, giving correlation coefficients of 0.69 for ERA-Interim and 0.61 for NCEP2.

414 Figure 8 shows that the two reanalyses represent tropical nights with less success, lower
415 correlations, than summer days (section 4.5.1). The histogram in Fig. 8a shows that the most frequent
416 correlation values range between 0.4 and 0.7 for ERA-Interim while NCEP2 presents correlation values
417 less than 0.6 in the whole region (Fig. 8b). Figs. 8c and 8d show that the two reanalyses overestimate
418 tropical nights although ERA-Interim has smaller biases than NCEP2 toward the south (MBE of 20-40
419 days for ERA-Interim and MBE of 40-60 days for NCEP2). The histograms in Figs. 8e and 8f indicate that
420 ERA-Interim presents common RMSE between 20 and 40 days while the most frequent RMSEs for
421 NCEP2 are well above the 40 days.

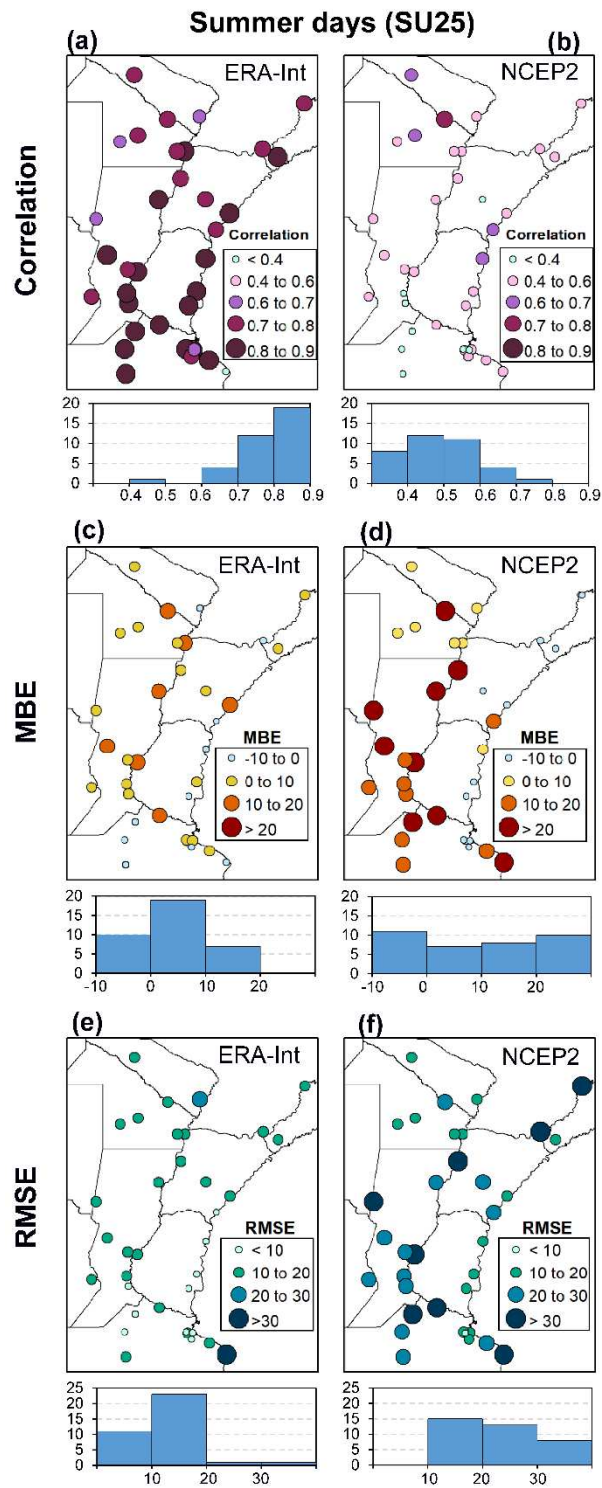
422 **4.5.3 Number of frost days (FD)**

423 As with the two previous indices, the number of frost days is largest towards the colder south.
424 Fig. 6c shows that both ERA-Interim and NCEP2 tend to reproduce the spatial mean fields, but
425 underestimate the spatiotemporal variability of frost days, particularly toward the south. Note that in
426 the northern portion of the region, closest to the tropics, there are less than 5 frost days per year (see
427 Fig. 6c), still, when they occur, they may severely damage crops that are of more subtropical nature.
428 The time series of area-averaged frost days on the right panel exhibit similar variability ($r = 0.86$ for
429 ERA-Interim and $r = 0.87$ for NCEP2) but with a systematic mean bias error of -3 days for NCEP2 and -5
430 days for ERA-Interim.

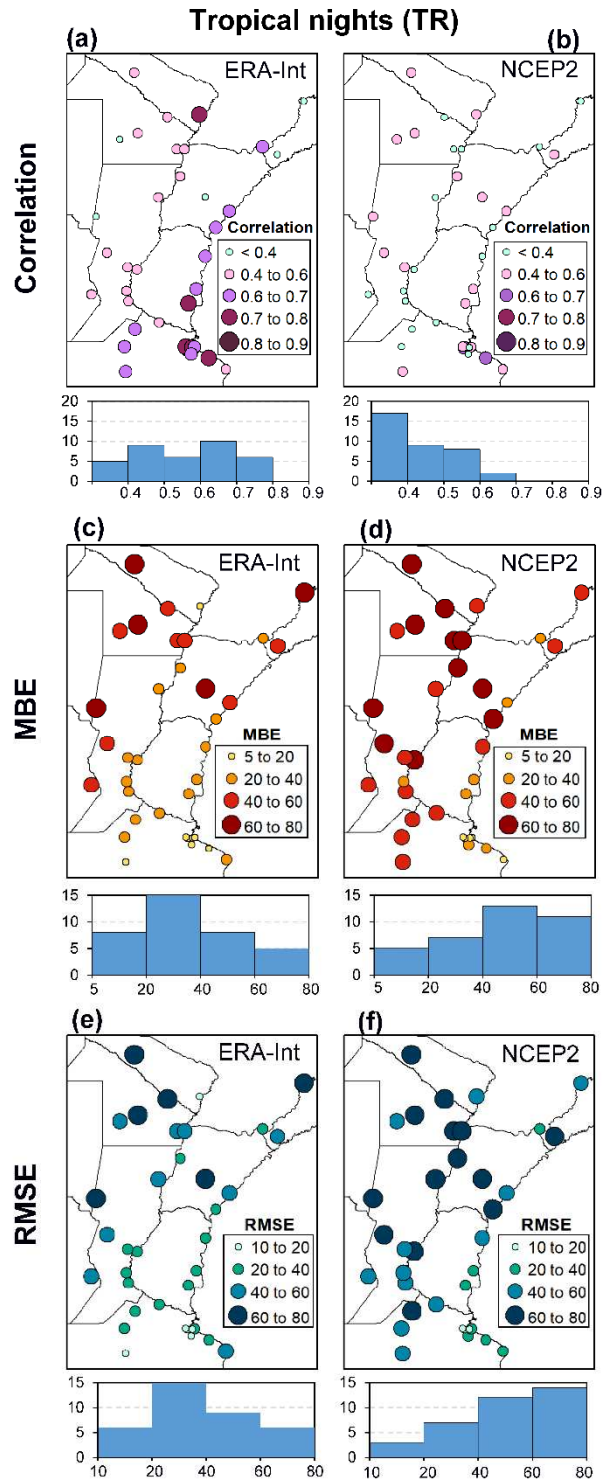
431 Figure 9 shows that the two reanalyses characterize frost days with similar statistical metrics:
432 the most frequent correlation coefficients range between 0.5 and 0.7 (Figs. 9a and 9b) and MBE reaches
433 values lesser than -5 days towards the south of the study region (Figs. 9c and 9d). This underestimation
434 represent almost 30% of the annual mean values of frost days towards the colder south, where both
435 reanalyses exhibit the highest RMSE values (Figs. 9f and 9g).



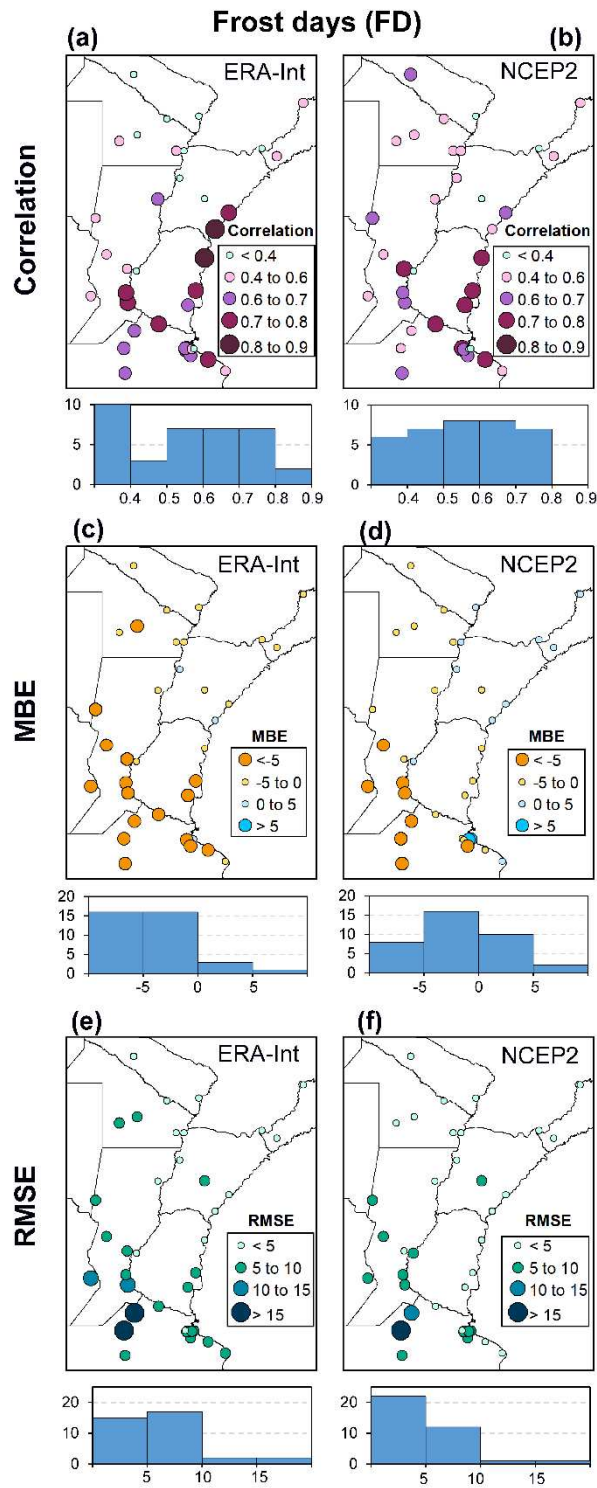
436 **Fig. 6. (a)** Summer days (SU25), **(b)** tropical nights (TR) and **(c)** frost days (FD) represented by the ERA-
 437 Interim and NCEP2 reanalyses for the period 1979-2011 and compared with observations. Spatial
 438 distribution of mean climatology values are given in the first two panels while area-averaged time series
 439 of the Argentinian territory in the third panel of each row.



440 **Fig. 7.** Spatial distribution of the correlation coefficients (a, b), the MBE (c, d) and the RMSE (e, f) for
 441 summer days (SU25) represented by the ERA-Interim and NCEP2 reanalyses for the period 1979-2011.
 442 Histograms are provided below of each map.



443 **Fig. 8.** Spatial distribution of the correlation coefficients (a, b), the MBE (c, d) and the RMSE (e, f) for
 444 tropical nights represented by the ERA-Interim and NCEP2 reanalyses for the period 1979-2011.
 445 Histograms are provided below of each map.



446 **Fig. 9.** Spatial distribution of the correlation coefficients (a, b), the MBE (c, d) and the RMSE (e, f) for
 447 frost days represented by the ERA-Interim and NCEP2 reanalyses for the period 1979-2011. Histograms
 448 are provided below of each map.

449 5. Precipitation-related climate extremes

450 5.1 Intense precipitation events

451 We characterize the intensity of precipitation-related climate extremes using two indices (see
452 Table 2): the annual maximum 1-day precipitation (RX1day) and the simple daily intensity index (SDII)
453 for precipitation, which is the average accumulated precipitation in rainy days. [The RX5day was also
454 studied, but is not shown due to its similarity to RX1day.]

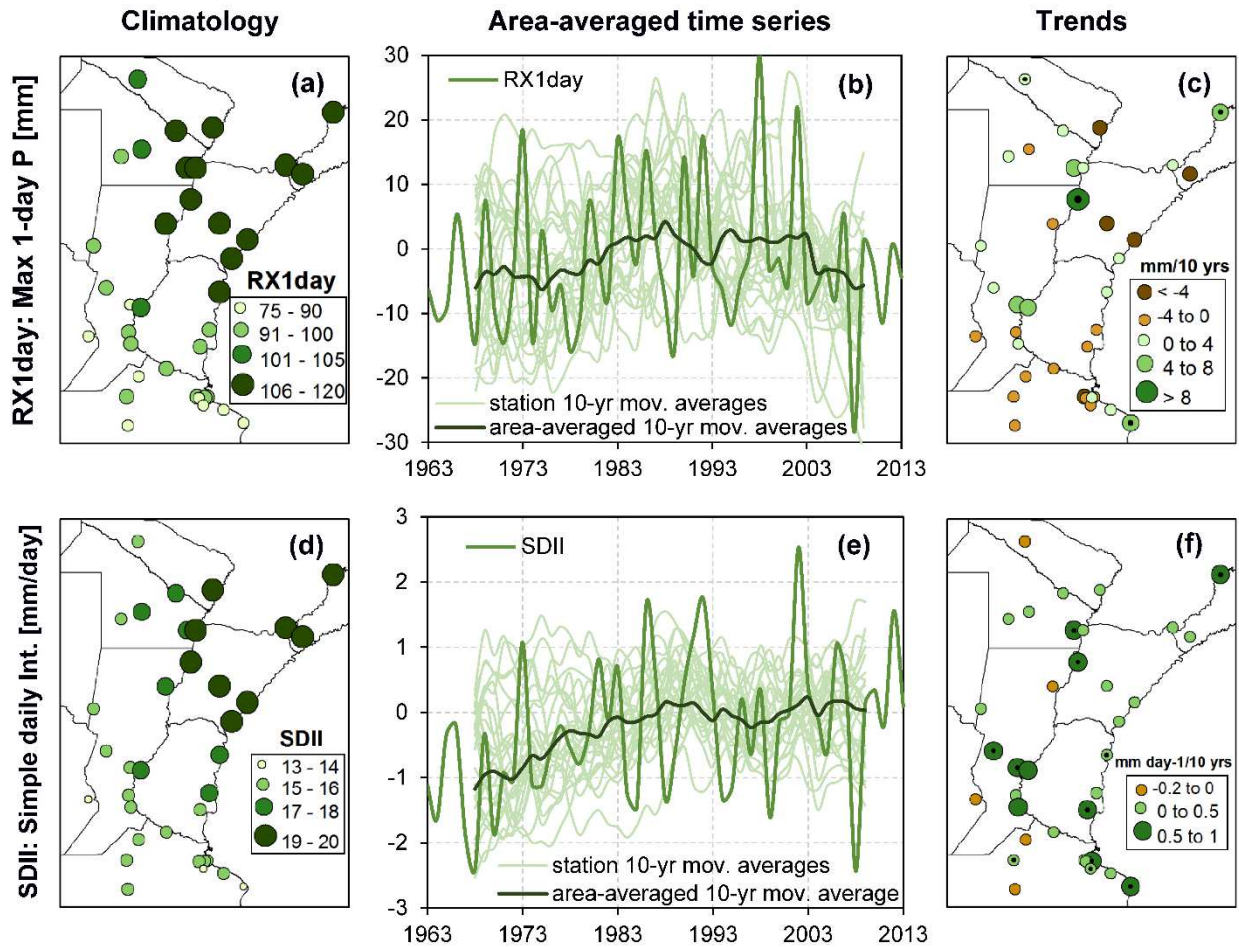
455 The spatial distribution of RX1day (Fig. 10a) has a spatial gradient increasing from the
456 southwest to the northeast that agrees with the annual mean precipitation fields (Fig. 1f). The
457 climatological values in Fig. 10a of RX1day range from 75 mm to 120 mm. The area-averaged evolution
458 of RX1day in Fig. 10b indicates that maximum 1-day precipitation events have increased from 1970 to
459 about 2000, declining slightly since mid-2000s. Note the large dispersion in the time series of all stations
460 (thin lines) that suggests a large spatial and temporal variability in intense precipitation events.
461 Particularly, NEA exhibits high interannual variability in intense precipitation events as shown by the
462 area-averaged time series of RX1day in Fig. 10b. The more intense events tend to occur during El Niño
463 years (e.g., 1998, 2002). Precipitation events during La Niña years (e.g., 1989, 2008) do not achieve the
464 same intensity. Table 4 presents ENSO-range periodicities for RX1day (a cycle of 3.6 years accounting
465 for 27% of its variance) and for RX5day (a noticeable 2.5-yr mode that explains 35% of the total index
466 variance). According to Fig. 10c, the annual maximum 1-day precipitation amounts present no definite
467 pattern of change, perhaps due to the fact that precipitation is highly variable in this region.

468 The simple daily intensity index presents the highest values in the wettest portion of NEA, i.e.
469 towards northeast (Fig. 10d). Although the SSA method does not extract trends with statistical
470 significance for the area-averaged SDII time series (Fig. 10e), the 10-yr moving averages series shows
471 that precipitation intensity has increased since the early 1970s to the present. Consistently, Fig. 10f
472 indicates that the increase occurred in the whole region, with 31 out of 36 stations showing positive
473 trends (11 of them significant at least at a 95% confidence level). The average change is about 1

474 mm/day in the last 50 years (see the time series of the area-averaged 10-yr moving average in Fig. 10e),
 475 with some areas showing increases of up to 1 mm/day per decade (see Fig. 10f). As in the case of
 476 RX1day index, the high dispersion in the 10-yr moving averages time series of all stations (Fig. 10e)
 477 indicates that the changes in precipitation intensity are modulated by large spatiotemporal variability.
 478 In particular, Table 4 shows that SDII is strongly influenced by an interannual variability cycle of 5 years
 479 that explains 35% of its variance.

480 **Table 4.** Summary of the main variability modes of precipitation-related extremes found with SSA.

SSA Results of Precipitation-based Indices					
	Index	Index Name	Components	Trend or Dominant Period (year/cycle)	Explained variance (%)
Intensity	RX1day	Max 1-day precipitation	T-PC1 and T-PC2	3.6	27
	RX5day	Max 5-day precipitation	T-PC1 and T-PC2	2.5	35
	SDII	Simple daily intensity index	T-PC1 and T-PC2	5	35
Duration	CWD	Consecutive wet days	No significant modes		
	CDD	Consecutive dry days	No significant modes		



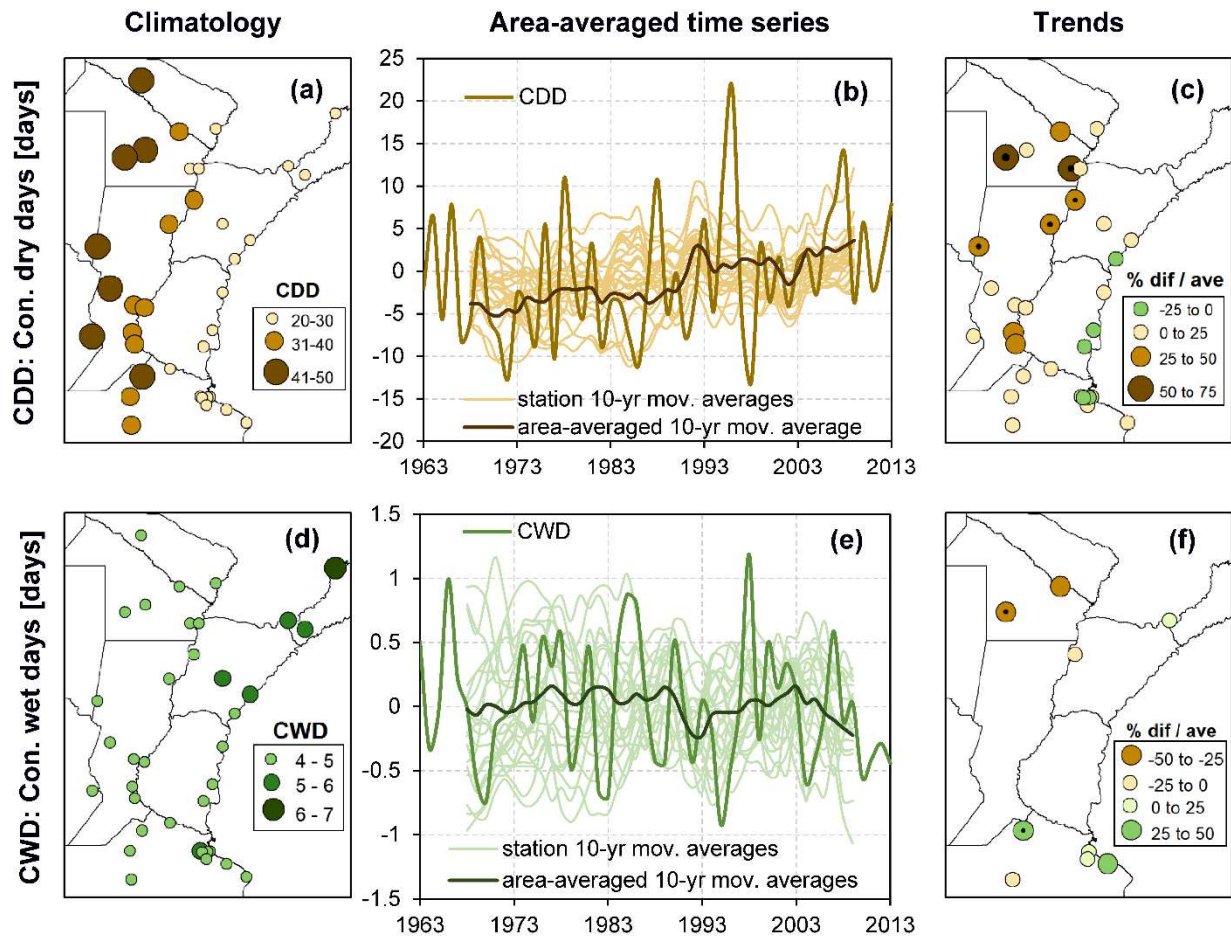
481 **Fig. 10:** Intense precipitation climate extremes characterized by the annual maximum 1-day
 482 precipitation amount (RX1day; **a-c**) and the simple daily intensity index (SDII, **d-f**). Left panels (**a, d**):
 483 climatological mean values in the 1963-2013 period. Middle panels (**b, e**): the temporal evolution of
 484 the anomalies of the area-averaged indices and their trends. Right panels (**c, f**): the spatial
 485 distribution of linear trends. Green colors indicate a shift toward wetter conditions while brown colors
 486 toward drier conditions. Station highlighted with a black dot indicate a significant linear trend, at
 487 least at the 95% confidence level. The definition of each index is given in Table 2. The units of each
 488 index is shown in brackets.

489 **5.2 Duration of wet and dry spells**

490 Figure 11 presents the maximum annual duration of dry and wet spells as characterized by the
491 consecutive dry/wet days indices (CDD and CWD; see Table 2 for definitions). It is noted that wet spells
492 refer to precipitation events and do not consider hydrological aspects (longer term flooding) due to
493 recurring non-consecutive wet spells.

494 The climatology in Fig. 11a reveals a longitudinal spatial gradient ranging from 20-30
495 consecutive dry days in the east and increasing westwards to almost 50 days. This spatial gradient
496 agrees with the precipitation climatology field (see Fig. 1f). Figs. 11b and 11c indicate that dry spell
497 duration has increased in recent decades. Fig. 11b shows a continuous increase of dry spell duration
498 over the whole region since the 1970s (see the time series of the area-averaged 10-yr moving average),
499 also influenced by a high interannual variability. Fig. 11c shows a homogeneous pattern of change with
500 27 stations with positive trends (75% of the total observed stations) increasing the duration of dry spells
501 by 1 to 5 dry days per decade. Notably, the largest increases occurred towards the north, where 5
502 locations have positive trends that exceed the confidence level of 95%.

503 Characteristics of the wet spells presented in Figs. 11d-e show that their duration is shorter
504 than for dry spells: wet spells tend to last 4 to 5 days in most of the study region, although up to 7
505 consecutive wet days can occur towards the rainiest northeastern sector (Fig. 11d). Fig. 11e shows high
506 interannual variability of wet spell anomalies with no noticeable trend. As seen in Fig 11f, the spatial
507 pattern of trends lacks adequate information, with few non-significant trends and the rest having no
508 changes (and thus not plotted).



509 **Fig. 11.** Duration of wet and dry spells characterized by the annual consecutive dry days (CDD; a-c)
 510 and the consecutive wet days (CWD, d-f). Left panels (a, d): climatological mean values in the 1963-
 511 2013 period. Middle panels (b, e): the temporal evolution of the anomalies of the area-averaged
 512 indices and their trends. Right panels (c, f): the spatial distribution of linear trends computed in
 513 percentage units as the ratio between the linear trend in the 51 years analyzed and the temporal
 514 average in the same period for each station. Green colors indicate a shift toward wetter conditions
 515 while brown colors toward drier conditions. Station highlighted with a black dot indicate a significant
 516 linear trend, at least at the 95% confidence level. The definition of each index is given in Table 2. The
 517 units of each index is shown in brackets.

518 **5.3 Precipitation-related extremes in reanalyses**

519 The ability of the global reanalyses to represent precipitation-related extremes is evaluated for
520 the annual maximum consecutive 5-day precipitation amount (RX5day) and the maximum annual
521 number of consecutive dry days (CDD). RX5day is similar to RX1day discussed in section 5.1, with the
522 only difference that it considers amounts in five days instead of one, thus allowing for more stable
523 results.

524 **5.3.1 Maximum 5-day precipitation amount (RX5day)**

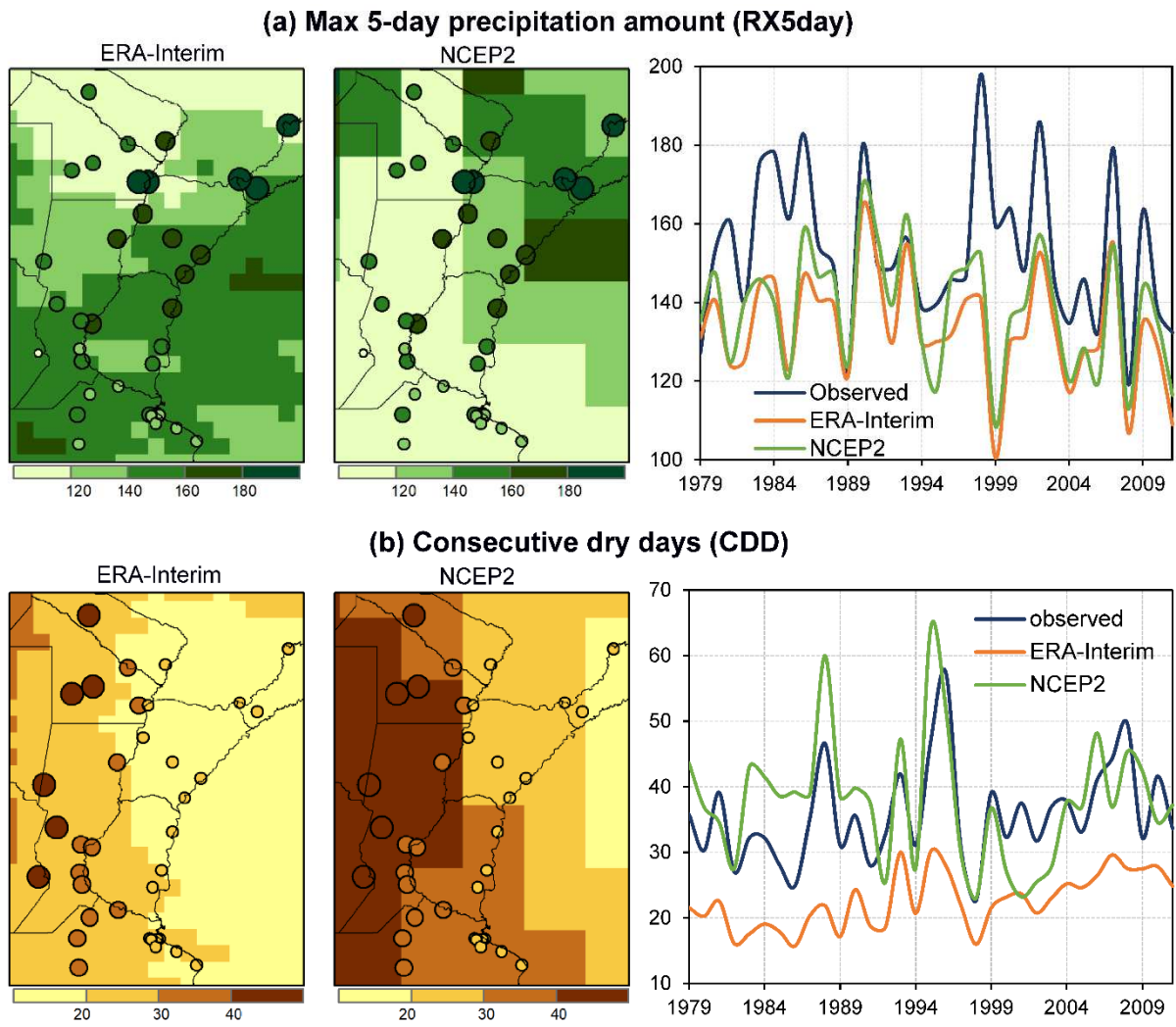
525 According to Fig. 12a, the observed climatology of RX5day (circles) presents a southwest-
526 northeast gradient that ranges from 125 mm to 200 mm with high spatial variability. Both reanalysis
527 climatologies depict a smoothed version of the observed spatial variability. However, the reanalyses
528 reproduce the temporal variability of the observed RX5day, achieving correlation coefficients close to
529 0.65. Yet, there are periods (1998-2000) in which large departures are found. The time series show that
530 ERA-Interim and NCEP2 underestimate the time evolution of area-averaged RX5day by about 16-18
531 mm, which represents relative errors of about 10-12% with respect to the area-averaged observations.

532 Figure 13 compares the spatial distribution of the RX5day for ERA-Interim and NCEP2 reanalyses
533 against in-situ observations. Both reanalyses fail to represent the observed RX5day, as their correlations
534 are lower than 0.2 in the whole region (Figs. 13a and 13b, respectively). The two reanalyses also
535 present dry biases of more than 40 mm toward the north of the study region (Figs. 13c and 13d). The
536 RMSE (Figs. 13e and 13f) are large throughout the study region, with more than 80% of the stations (30
537 out of 36) presenting RMSE values higher than 60 days (see histograms below the maps in Figs. 13e and
538 13f).

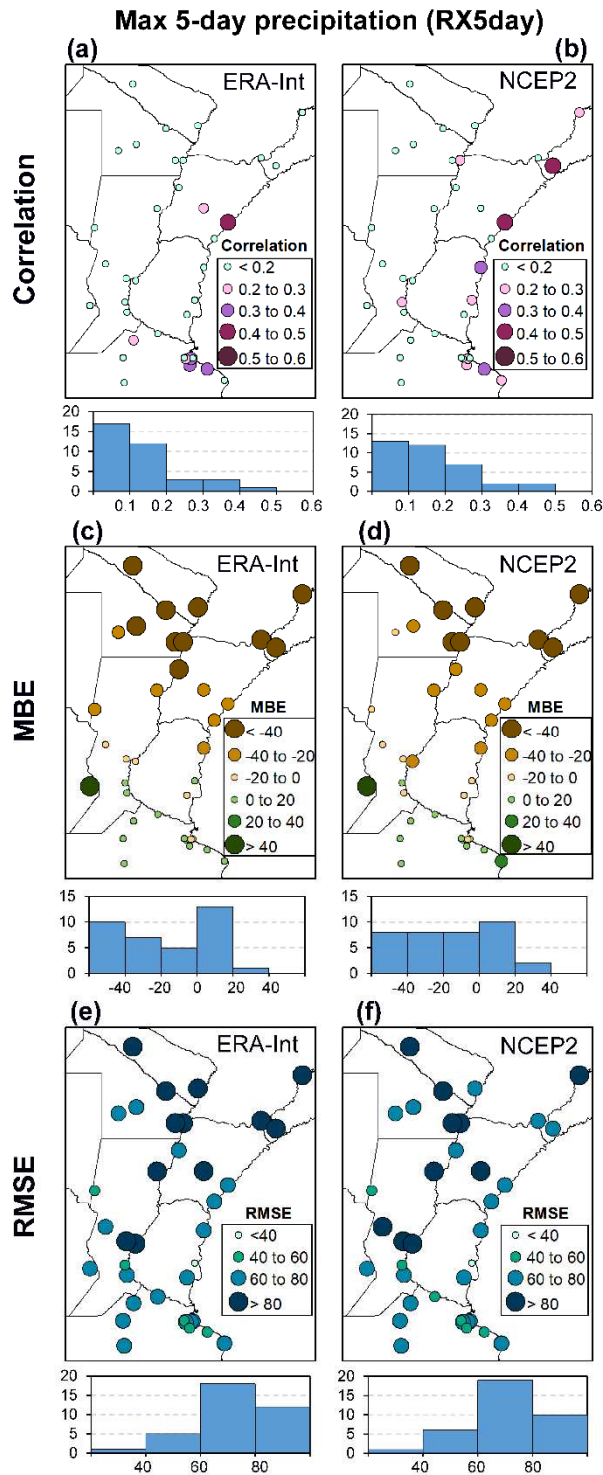
539 **5.3.2 Consecutive dry days (CDD)**

540 Figure 12b shows that the observed climatology of CDD (circles) presents a strong east-west
541 spatial gradient (discussed in section 5.2). Both reanalysis climatologies also display the east-west
542 gradient (shades) but the ERA-Interim underestimates the observed spatial variability while NCEP2
543 overestimates it. The area-averaged CDD time series have a similar evolution reaching correlation
544 coefficients close to 0.7. Consistently with the spatial behavior, ERA-Interim underestimates the
545 observed time variability with a mean bias error of 13 days (36% of the observed mean value in the
546 whole period) while NCEP2 overestimates the temporal evolution of CDD reaching a mean bias error of
547 2 days, which represents a 6% of the observed mean value.

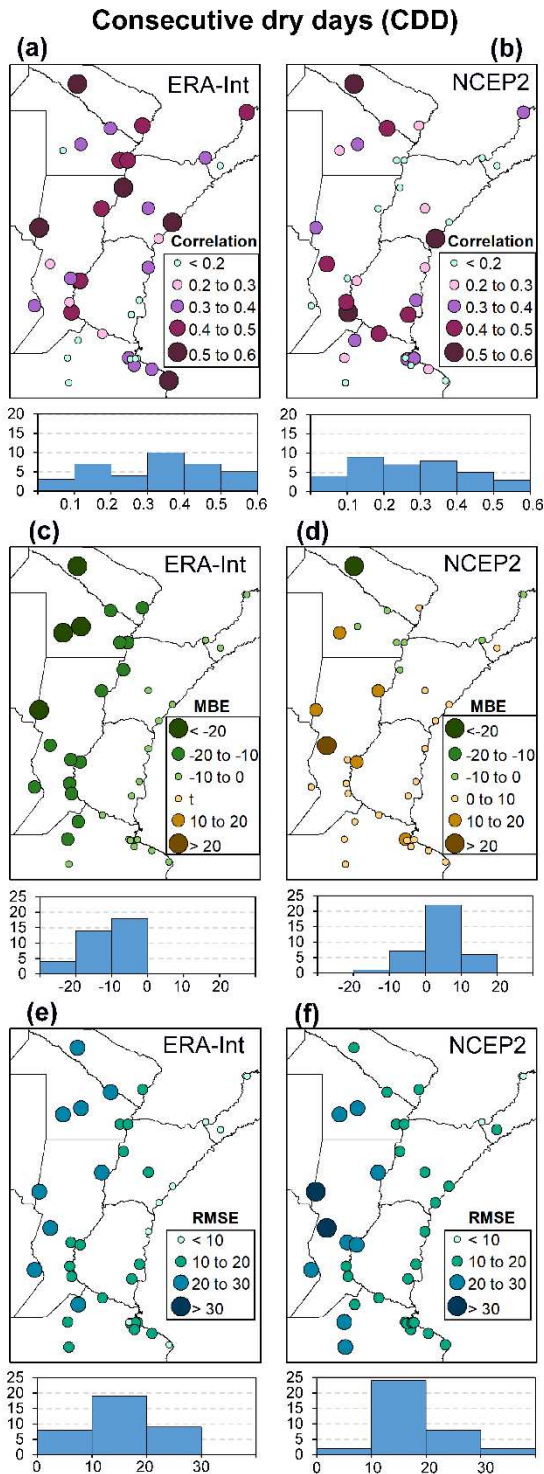
548 Figure 14 presents the evaluation of the CDD metrics, and a comparison of Fig. 14 and Fig. 13
549 indicates that both reanalyses performs better for CDD than for RX5day. ERA-Interim reproduces the
550 observed CDD with higher correlations than NCEP2, mainly toward the northern sector (Fig. 14a and
551 14b). As shown by Figs. 14c-f, both reanalyses present the highest biases toward the driest east: RMSE
552 acquires values higher than 20 days (Figs. 14e and 14f) but while ERA-Interim underestimates
553 observations (Fig. 14c), NCEP2 overestimates them (Fig. 14d). The histograms in Figs. 14c and 14d show
554 that ERA-Interim acquires frequent mean bias in the range $-20 < \text{MBE} < -10$ while NCEP2 most frequent
555 errors are in the range $0 > \text{MBE} > 10$, suggesting that the ERA-Interim underestimation is higher than
556 the NCEP2 overestimation.



557 **Fig. 12.** Intense precipitation events characterized by the annual maximum 5-day precipitation
 558 amount (RX5day, **a**) and short-term droughts represented by the annual maximum consecutive
 559 dry days (CDD, **b**) represented by the ERA-interim and NCEP2 reanalyses for the period 1979-2011
 560 and compared with observations. Spatial distribution of mean climatology values are given in the
 561 first two panels while area-averaged time series in the third panel of each row.



562 **Fig. 13.** Spatial distribution of the correlation coefficients, the MBE and the RMSE for maximum 5-
 563 day precipitation (RX5day) represented by the ERA-Interim and NCEP2 reanalyses for the period
 564 1979-2011. Histograms are provided below of each map.



565 **Fig. 14.** Spatial distribution of the correlation coefficients, the MBE and the RMSE for the annual
 566 maximum consecutive dry days (CDD) represented by the ERA-Interim and NCEP2 reanalyses for
 567 the period 1979-2011. Histograms are provided below of each map.

568 6. Discussion

569 6.1 Changes in extreme events and potential impacts

570 The results show that minimum-temperature extremes had a clear signal of nighttime warming
571 due to a significant increase in warm nights and a concurrent significant decrease in cold nights.
572 Maximum-temperature extremes also exhibited a daytime warming resulting from a significant increase
573 in warm days and a significant decrease in cold days. While the minimum temperature warming seems
574 to have been stabilizing in recent decades, the maximum temperature warming continues to rise.
575 According to literature, these changes may have agricultural implications as the decrease in cold nights
576 shortens crops' critical growth periods reducing wheat and barley yields (Magrin et al., 2009; García et
577 al., 2015). On the other hand, the increase of warm days affect the critical growth periods of maize and
578 sunflower in summer, while the decrease of cold days may reduce the flowering and yield of winter
579 wheat (Magrin et al., 2012).

580 The results also suggest that the region is experiencing longer and more frequent warm spells
581 than cold spells. The longer duration of heat waves may have important impacts on the population,
582 increasing their mortality risk by heat strokes and producing more frequent collapses of energy systems
583 (Magrin et al., 2014). In agriculture, the yields of maize and sunflower can be reduced because their
584 critical periods are very sensitive to the summer high temperatures (Rondanini et al., 2006; Mayer et
585 al., 2012).

586 The increased intensity of heavy precipitation events in the last decades over the whole NEA
587 constitutes a growing risk for urban settlements where heavy rainfall may exceed the capacity of
588 drainage systems, causing significant infrastructure losses and, in the most extreme cases, deaths
589 (Barros et al., 2015; Lovino, 2015). Intense precipitation events in the predominantly flat agricultural
590 plains lead to extensive waterlogging with important economic impacts due to loss of crops and
591 decreased livestock productivity. While precipitation has increased, dry spells in recent decades have

592 tended to last longer, suggesting that more persistent short-term droughts may affect agriculture
593 activities, mainly in the drier area towards the northwest.

594 **6.2 Large-scale climate factors and the changes and variability in NEA climate extremes**

595 The South American climate underwent a transition in the 1970s, linked to the 1976–77 global
596 climate shift, which strongly affected the South American Monsoon System (Carvallo et al., 2011). It has
597 been speculated that several large-scale climate-forcing factors could have combined to cause this
598 change, including a cold-to-warm sea surface temperature shift in the tropical Pacific Ocean (Huang et
599 al., 2005; Jacques-Coper and Garreaud, 2015) and a multidecadal cooling in the tropical Atlantic Ocean
600 (Seager et al., 2010; Barreiro et al., 2014). This climate shift appears to have been a source of change for
601 trends and variability in precipitation, river streamflow and temperature in several regions of South
602 America (e.g., Marengo, 2004; Kayano et al., 2009; Castino et al., 2016). Agosta and Companucci (2008)
603 reported that the wetter conditions could have been influenced by the 1976-1977 climate shift that
604 reduced the cyclonic activity at mid-latitudes together with a stronger northerly flow, which brings in
605 higher humidity levels from northeastern Argentina. In this context, our results suggesting that intense
606 precipitation events and minimum temperature extremes experienced long-term increases since the
607 1970s in northeastern Argentina, are in agreement with Cavalcanti et al. (2015) and Carril et al. (2016).

608 Extremes of minimum temperature (cold and warm nights) showed a stabilization in their
609 trends since the 1980s. Rusticucci et al. (2016) proposed that these trends could be influenced by a shift
610 towards the west of the South Atlantic anticyclone together with an increase in the north component of
611 the wind measured by the meridional wind at 925 hPa in central Argentina that occurred during 1970s
612 and 1980s being stabilized during the 1990s and 2000s.

613 Other changes seem to have occurred since the 2000s. This study shows that some of the
614 observed increases in precipitation and minimum temperature extremes seem to have stabilized in

615 recent decades in northeastern Argentina. We showed that the magnitude of intense precipitation
616 events appears to be stabilizing in the last decade or so. The stabilization of the long-term wetting trend
617 has been discussed in recent years (e.g., Seager et al., 2010; Barreiro et al., 2014; Lovino et al., 2014).
618 These authors suggested that a cold phase of the Atlantic Multidecadal Oscillation (AMO) may have
619 favored wet anomalies in decadal time scales between 1970s and 2000s over NEA while the reversal in
620 the wetting trend could be associated to a shifting toward a warm phase of the AMO (Li et al., 2018)
621 that may have forced a long-term decrease in precipitation during the late 2000s.

622 Our results suggest that the interannual variability significantly affects minimum-temperature
623 and intense precipitation extremes in northeastern Argentina (in agreement with Rusticucci et al., 2012
624 and Carril et. al, 2016). Interestingly, minimum-temperature extremes (including frost days) showed a
625 significant interannual cycle of 4 years. Recently, Lovino et al. (2018) found that regional minimum
626 temperature can be related to ENSO with a periodicity of roughly 4 years. It is well known that the
627 number of frost days in northeastern Argentina is highly influenced by the ENSO phenomenon: less
628 frost days are observed during El Niño years and more are found during La Niña years (Müller et al.,
629 2000; Müller et al., 2003). In consonance with that, our results suggest that nighttime temperature
630 extreme events might be also affected by the ENSO in this frequency. There is much evidence that
631 ENSO modulates the interannual variability of extreme precipitation events over northeastern
632 Argentina (e.g., Haylock et al., 2006; Grimm and Tedeschi, 2009; Cavalcanti, 2012). Our results suggest
633 that extreme values of the area-averaged time series of RX1day and RX5day are associated to ENSO
634 conditions. Consistently, the main significant periodicities of the intense precipitation events of one day
635 and five days (3.6 and 2.5 years) found in this study were also reported in the ENSO SST pattern (Moron
636 et al., 1998; Lovino et al., 2018) and ENSO indices (e.g., Wolter and Timlin, 2011).

637 **6.3 The skill of NCEP2 and ERA-Interim reanalyses to represent NEA climate extremes**

638 The ERA-Interim is a newer reanalysis that unlike the older NCEP2 includes assimilation of
639 surface temperature observations. Our findings are in line with this information, as they show that ERA-
640 Interim exhibits greater ability to reproduce the spatial and temporal variability of summer days than
641 NCEP2 over the study region. NCEP2 and ERA-Interim tend to represent maximum-temperature
642 extremes (here characterized by summer days) better than minimum-temperature extremes (as
643 represented by tropical nights and frost days). This result is consistent with Rusticucci and Kousky
644 (2002) and Zaninelli et al. (2015) who showed similar differences between NCEP and ERA40. Both
645 reanalyses represent the interannual variability of tropical nights and frost days, although with
646 significant positive systematic errors for tropical nights even for the ERA-Interim that assimilates
647 observed temperature. Still, NCEP2 fails to reproduce the spatial patterns of both summer days and
648 tropical nights and both reanalysis have closer values among themselves than with observations. Frost
649 days exhibit negative mean bias errors, which intriguingly are larger for ERA-Interim. In summary, while
650 the reanalyses can reproduce the interannual variability of temperature-related climate extremes,
651 magnitudes are off, particularly for tropical nights.

652 Precipitation-related extreme events are more difficult to reproduce by reanalysis products. The
653 two reanalyses were able to recognize the time evolution of area-averaged intense precipitation events
654 in the last decades, but smooth out the spatial distribution of these events. The RX5day is represented
655 with significant dry biases towards the north of the study region. These results agree with Boers et al.
656 (2015), who reported that ERA-Interim fail to reproduce large convective systems in southeastern South
657 America, and Silva et al. (2011) and Albuquerque de Almeida et al. (2018), who found that NCEP2
658 presents dry biases and difficulties to simulate the intensity of precipitation. The two reanalyses
659 recognized dry spells patterns as characterized by CDD, although NCEP2 tends to represent longer dry
660 spells, and ERA-Interim shorter dry spells compared to observations. Thus, our results suggest that
661 reanalyses products have limits that should be taken carefully into account if they are included in

662 studies that involve changes in climate extremes in northeastern Argentina, particularly for
663 precipitation-related extremes.

664 **7. Concluding remarks**

665 This paper has investigated the variability and changes in daily climate extreme events during
666 the last five decades in the fertile northeast region of Argentina. The extremes include warm and cold
667 days and nights, temperature diurnal amplitude, frost days, heat and cold waves, intense precipitation
668 events and dry and wet spells. The intensity, duration and frequency of temperature- and precipitation-
669 related climate extremes were studied using 15 indices of the core set of ETCCDI indices, selected
670 according to their capacity to represent relevant extreme events in the study region. We also assessed
671 the ability of the ERA-Interim and NCEP2 reanalyses to reproduce the observed variability of climate
672 extremes during the period 1979-2011.

673 The changes in daily temperature extremes reveal a trend towards warmer conditions over
674 northeastern Argentina, which is consistent with what has been observed in other regions of the world
675 (e.g., Seneviratne et al., 2012; Donat et al., 2013). This warming is revealed as an increase of warm days
676 and warm nights, as well as a decrease of cold days and cold nights. Although the number of cold nights
677 declined following the general warming trend in the region, the number has not changed significantly
678 since 1980. The number of frost days exhibits large interannual and decadal variability without
679 noticeable trends. The diurnal amplitude of temperature in winter has been increasing since about
680 2000, possibly as a result of the decrease in cold days, i.e., those days with maximum temperature
681 lesser than the 10th percentile, and despite the lack of changes in the number of cold nights.

682 Heat and cold waves also reflect the general warming in NEA. Firstly, heat waves almost double
683 the frequency and duration of cold waves. Second, during recent decades heat waves have tended to
684 increase their duration and cold waves tended to be less persistent in time. The occurrence of longer
685 heat waves is also related to changes in precipitation features noted in the trend towards longer dry

686 spells. These results agree with Seneviratne et al. (2012) who showed that the longer persistence of dry
687 days during warm seasons contributes to higher temperatures and more extended duration of heat
688 waves. Our results showed that heat waves are more frequent and persistent towards the west, where
689 dry spells persist longer, with events reaching up to 50 days without rain.

690 Daily precipitation intensities in the range of 13-20 mm day⁻¹ are common in NEA. However, in
691 occasions, extreme precipitation events can exceed 100 mm in one day and 200 mm in five days,
692 particularly towards the wetter northeast. Our results show that intense precipitation events are highly
693 influenced by interannual variability and, although no significant trends have been found with the SSA
694 method, a steady increase of mean intensity values occurred since 1970. Since the region is mostly flat
695 and has several important rivers, the increased intensity of extreme precipitation events has led to
696 severe floods affecting agriculture and human settlements. The annual maximum amount of 1-day and
697 5-day precipitation events also increased since 1970, although it seems to be stabilizing in recent years,
698 as discussed above. The observed high variability is influenced by frequent and intense mesoscale
699 convective systems and convective storms (Zipser et al., 2006; Rasmussen et al., 2016) that cause
700 extreme precipitation events everywhere in the region. The prevalence for few days of convective
701 systems and convective storms also explains the short duration of consecutive wet days. Wet spells do
702 not persist for more than 5-6 days in average. However, during those days large amounts of
703 precipitation can accumulate leading to severe floods (Cavalcanti, 2012).

704 Finally, the ERA-Interim and NCEP2 reanalyses have different degrees of success in representing
705 the observed extreme temperature and precipitation events. ERA-Interim can recognize the evolution
706 of temperature extremes as number of summer days and tropical nights in time and space although
707 with biases in magnitude. NCEP2 has a similar behavior for the area-averaged time evolution, but poor
708 correlations are found at individual stations.

709 The two reanalyses represent extreme precipitation events with large biases, which are
710 particularly noticeable when looking at the performance locally at each station. Although both

711 reanalyses tend to recognize the variability of the area-averaged annual 5-day maximum precipitation
712 in time, they underestimate the representation of their spatial distribution, mainly in the wetter
713 northeast. Despite the large biases, the two reanalyses can represent better the short-term drought
714 characterized by the annual maximum consecutive dry days than the extreme precipitation events
715 represented by annual 5-day maximum precipitation. In general, reanalyses perform better for
716 temperature extremes than for precipitation extremes. Although reanalyses would be expected to add
717 information for climate extremes in areas of scarce observations like northeastern Argentina, they still
718 need to be used with great caution and as a complement to observations.

719 **Acknowledgements**

720 We are grateful to the anonymous reviewers whose constructive comments and
721 recommendations helped to improve the manuscript. This research was carried out with support of
722 Projects CRN3035 and CRN3095 of the Inter-American Institute for Global Change Research (IAI), which
723 is supported by the US National Science Foundation. NOAA Grant NA14NES4320003 and a UNL Project
724 C.A.I. + D. 2011 35/180 are also acknowledged. Miguel Lovino and Omar Müller were supported by
725 fellowships from CONICET, Argentina. The NCEP2 climate indices were provided by the Canadian Centre
726 for Climate Modelling and Analysis from the archive website <http://www.cccma.ec.gc.ca/data/climdex/>
727 (Sillman et al., 2013).

728 **References**

- 729 Agosta, E. A., Compagnucci, R.H., 2008. The 1976/77 austral summer climate transition effects on the
730 atmospheric circulation and climate in Southern South America. *J. Clim.* 21, 4365–4383.
731 DOI:10.1175/2008JCLI2137.1
- 732 Albuquerque de Almeida, V., Marton, E. and Nunes, A. M. B., 2018. Assessing the ability of three global
733 reanalysis products to reproduce South American monsoon precipitation. *Atmósfera* 31(1), 1-10.
734 DOI: 10.20937/ATM.2018.31.01.01
- 735 Alexander, L. V., Zhang, X., Peterson, T. C., Caesar, J., Gleason, B., Klein Tank, A. M., Haylock, M., Collins,
736 D., Trewin, B., Rahimzadeh, F., Tagipour, A., Rupa Kumar, K., Revadekar, J., Griffiths, G., Vincent, L.,
737 Stephenson, D. B., Burn, J., Aguilar, E., Brunet, M., Taylor, M., New, M., Zhai, P., Rusticucci, M.,
738 Vazquez-Aguirre, J. L., 2006. Global observed changes in daily climate extremes of temperature and
739 precipitation. *Journal of Geophysical Research-Atmospheres* 111, D05109. DOI:
740 10.1029/2005JD006290.
- 741 Barreiro, M., Diaz, N. Renom, M., 2014. Role of the global oceans and land–atmosphere interaction on
742 summertime interdecadal variability over northern Argentina. *Climate Dyn.*, 42, 1733-1753. DOI:
743 10.1007/s00382-014-2088-6.
- 744 Barros, V., Doyle, M., Camilloni, I., 2008. Precipitation trends in southeastern South America:
745 Relationship with ENSO phases and with low-level circulation. *Theor. Appl.Climatol.*, 93, 19–33.
746 <https://doi.org/10.1007/s00704-007-0329-x>
- 747 Barros, V. R., Boninsegna, J. A., Camilloni, I. A., Chidiak, M., Magrín, G. O. and Rusticucci, M., 2015.
748 Climate change in Argentina: trends, projections, impacts and adaptation. *WIREs Clim Change*, 6:
749 151–169. DOI:10.1002/wcc.316

750 Barrucand, M., Rusticucci, M. and Vargas, W., 2008. Temperature extremes in the south of South
751 America in relation to Atlantic Ocean surface temperature and Southern Hemisphere circulation, J.
752 Geophys. Res., 113, D20111, DOI: 10.1029/2007JD009026.

753 Berbery, E.H., Collini, E.A., 2000. Springtime precipitation and water vapor flux over southeastern South
754 America. Mon. Wea. Rev., 128, 1328–1346, doi:10.1175/1520-0493(2000)128,1328:
755 SPAWVF.2.0.CO;2.

756 Berbery, E. H., Barros, V. R., 2002. The hydrologic cycle of the La Plata basin in South America. Journal of
757 Hydrometeorology, 3(6), 630-645. DOI: 10.1175/1525-7541(2002)003<0630:THCOTL>2.0.CO;2

758 Boers, N., Bookhagen, B., Marengo, J., Marwan, N., von Storch, J., Kurths, J., 2015. Extreme Rainfall of
759 the South American Monsoon System: A Dataset Comparison Using Complex Networks. J. Climate,
760 28, 1031–1056, DOI: 10.1175/JCLI-D-14-00340.1

761 Bronaugh, D., Werner, A., 2013. Zhang + Yue- Pilon trends package, Package “Zyp” version 0.10-1.
762 License LGPL-2.1, URL <http://r-project.org>.

763 Carbajo, A. E., Cardo, M. V., Vezzani, D., 2012. Is temperature the main cause of dengue rise in non-
764 endemic countries? The case of Argentina. International Journal of Health Geographics, 11, 26,
765 DOI: 10.1186/1476-072X-11-26.

766 Carril, A.F., Cavalcanti, I. F. A., Menéndez, C. G., Sörensson, A., López-Franca., N., Rivera, J., Robledo, F.,
767 Zaninelli, P., Ambrizzi, T., Penalba, O., da Rocha, R., Sánchez, E., Bettolli, M., Pessacg, N., Renom,
768 M., Ruscica, R., Solman, S., Tencer, B., Grimm, A., Rusticucci, M., Cherchi, A., Tedeschi, R., Zamboni,
769 L., 2016. Extreme events in the La Plata basin: a retrospective analysis of what we have learned
770 during CLARIS-LPB project. Climate Research 68: 95-116. DOI: 10.3354/cr01374.

771 Carvalho, L. M. V., Jones, C., Silva, A. E., Liebmann, B., Silva Dias, P.L., 2011. The South American
772 Monsoon System and the 1970s climate transition. Int. J. Climatol. 31, 1248–1256.
773 DOI:10.1002/joc.2147

774 Carvalho L.M.V., Cavalcanti I.F.A., 2016. The South American Monsoon System (SAMS). In: de Carvalho
775 L., Jones C. (eds) *The Monsoons and Climate Change*. Springer Climate. Springer, Cham DOI:
776 10.1007/978-3-319-21650-8_6.

777 Castino, F., Bookhagen, B., Strecker, M.R., 2016. River-discharge dynamics in the Southern Central
778 Andes and the 1976–77 global climate shift. *Geophys. Res. Lett.* 43. DOI: 10.1002/2016GL070868

779 Cavalcanti, I. F. A., 2012. Large scale and synoptic features associated with extreme precipitation over
780 South America: a review and case studies for the first decade of the 21st century. *Atmos. Res.* 118,
781 27–40. doi:10.1016/j.atmosres.2012.06.012.

782 Cavalcanti, I. F. A., Carril, A. F., Penalba, O. C., Grimm, A.M., Menéndez, C.G., Sanchez, E., Chechi, A.,
783 Sörensson, A., Robledo, F., Rivera, J., Pántano, V., Betolli, L. M., Zaninelli, P., Zamboni, L., Tedeschi,
784 R.G., Dominguez, M., Ruscica, R., Flach, R., 2015. Precipitation extremes over La Plata Basin—
785 review and new results from observations and climate simulations. *Journal of Hydrology* 523:
786 211–230. DOI: 10.1016/j.jhydrol.2015.01.028

787 CCSP, 2008: *Weather and Climate Extremes in a Changing Climate. Regions of Focus: North America,*
788 *Hawaii, Caribbean, and U.S. Pacific Islands. A Report by the U.S. Climate Change Science Program*
789 *and the Subcommittee on Global Change Research.* [Thomas R. Karl, Gerald A. Meehl, Christopher
790 D. Miller, Susan J. Hassol, Anne M. Waple, and William L. Murray (eds.)]. Department of
791 Commerce, NOAA’s National Climatic Data Center, Washington, D.C., USA, 164 pp.

792 Dee, D. P., Uppala, S. M., Simmons, A. J., Berrisford, P., Poli, P., Kobayashi, S., Andrae, U., Balmaseda, M.
793 A., Balsamo, G., Bauer, P., Bechtold, P., Beljaars, A. C. M., van de Berg, L., Bidlot, J., Bormann, N.,
794 Delsol, C., Dragani, R., Fuentes, M., Geer, A. J., Haimberger, L., Healy, S. B., Hersbach, H., Hólm, E.
795 V., Isaksen, I., Kållberg, P., Köhler, M., Matricardi, M., McNally, A. P., Monge-Sanz, B. M.,
796 Morcrette, J.-J., Park, B.-K., Peubey, C., de Rosnay, P., Tavolato, C., Thépaut, J.-N. and Vitart, F.,
797 2011. The ERA-Interim reanalysis: configuration and performance of the data assimilation system.
798 *Q.J.R. Meteorol. Soc.*, 137: 553–597. doi:10.1002/qj.828

799 Déqué, M., 2012. Continuous variables. In *Forecast Verification – A Practitioner’s Guide in Atmospheric*
800 *Science*, 2nd edn, Jolliffe IT, Stephenson DV (eds). John Wiley and Sons: Chichester, UK, 97–120.

801 Donat, M. G., Alexander, L., Yang, H., Durre, I., Vose, R., Caesar, J., 2013. Global Land-Based Datasets for
802 Monitoring Climatic Extremes. *Bull. Amer. Meteor. Soc.*, 94, 997–1006. DOI: 10.1175/BAMS-D-12-
803 00109.1

804 ECLAC (Economic Commission for Latin America and the Caribbean), 2015. The economics of climate
805 change in Latin America and the Caribbean Paradoxes and challenges of sustainable development.
806 United Nations, Santiago, Chile.
807 http://repositorio.cepal.org/bitstream/handle/11362/37311/S1420655_en.pdf

808 Fernández-Long, M. E., Müller, G. V., Beltrán-Przekurat, A. and Scarpatti, O. E., 2013. Long-term and
809 recent changes in temperature-based agroclimatic indices in Argentina. *Int. J. Climatol.*, 33: 1673–
810 1686. DOI: 10.1002/joc.3541

811 Field, C.B., V.R. Barros, K.J. Mach, M.D. Mastrandrea, M. van Aalst, W.N. Adger, D.J. Arent, J. Barnett, R.
812 Betts, T.E. Bilir, J. Birkmann, J. Carmin, D.D. Chadee, A.J. Challinor, M. Chatterjee, W. Cramer, D.J.
813 Davidson, Y.O. Estrada, J.-P. Gattuso, Y. Hijikata, O. Hoegh-Guldberg, H.Q. Huang, G.E. Insarov, R.N.
814 Jones, R.S. Kovats, P. Romero-Lankao, J.N. Larsen, I.J. Losada, J.A. Marengo, R.F. McLean, L.O.
815 Mearns, R. Mechler, J.F. Morton, I. Niang, T. Oki, J.M. Olwoch, M. Opondo, E.S. Poloczanska, H.-O.
816 Pörtner, M.H. Redsteer, A. Reisinger, A. Revi, D.N. Schmidt, M.R. Shaw, W. Solecki, D.A. Stone,
817 J.M.R. Stone, K.M. Strzepek, A.G. Suarez, P. Tschakert, R. Valentini, S. Vicuña, A. Villamizar, K.E.
818 Vincent, R. Warren, L.L. White, T.J. Wilbanks, P.P. Wong, and G.W. Yohe, 2014: Technical summary.
819 In: *Climate Change 2014: Impacts, Adaptation, and Vulnerability. Part A: Global and Sectoral*
820 *Aspects. Contribution of Working Group II to the Fifth Assessment Report of the Intergovernmental*
821 *Panel on Climate Change* [Field, C.B., V.R. Barros, D.J. Dokken, K.J. Mach, M.D. Mastrandrea, T.E.
822 Bilir, M. Chatterjee, K.L. Ebi, Y.O. Estrada, R.C. Genova, B. Girma, E.S. Kissel, A.N. Levy, S.

823 MacCracken, P.R. Mastrandrea, and L.L. White (eds.)]. Cambridge University Press, Cambridge,
824 United Kingdom and New York, NY, USA, pp. 35-94.

825 García, G.A., Dreccer, M. F., Miralles, D.J., Serrago, R. A., 2015. High night temperatures during grain
826 number determination reduce wheat and barley grain yield: a field study. *Glob Chang Biol.*, 21(11):
827 4153–4164. DOI: 10.1111/gcb.13009

828 Ghil, M., Vautard, R., 1991. Interdecadal oscillations and the warming trend in global temperature time
829 series. *Nature*, 350, 324-327. DOI: 10.1038/350324a0

830 Ghil, M., Allen, M., Dettinger, M. D., Ide, K., Kondrashov, D., Mann, M., Robertson, A., Saunders, A.,
831 Tian, Y., Varadi, F., Yiou, P., 2001. Advanced Spectral Method for Climatic Time Series. *Rev. of*
832 *Geop.*, 40, 1-41. DOI: 10.1029/2001RG000092

833 Guha-Sapir, D., Below, R., Hoyois, P., 2015. EM-DAT: International disaster database. Catholic University
834 of Louvain: Brussels, Belgium.

835 Grimm, A.M. and Tedeschi, R.G., 2009. ENSO and Extreme Rainfall Events in South America. *J. Climate*,
836 22, 1589–1609, DOI: 10.1175/2008JCLI2429.1.

837 Grimm, A. M., Laureanti, N. C., Rodakoviski, R. B., Gama, C. B., 2016. Interdecadal variability and
838 extreme precipitation events in South America during the monsoon season, *Climate Research*, 68,
839 277-294, DOI: 10.3354/cr01375.

840 Hardoy, J., Pandiella, G., 2009. Urban poverty and vulnerability to climate change in Latin America.
841 *Environment and Urbanization*, 21(1), 203-224. DOI: 10.1177/0956247809103019

842 Haylock, M. R, Peterson, T. C., Alves, L. M., Ambrizzi, T., Anunciação, Y. M. T., Baez, J., Barros, V. R.,
843 Berlato, M. A., Bidegain, M., Coronel, G., Corradi, V., Garcia, V. J., Grimm, A. M., Karoly, D.,
844 Marengo, J. A., Marino, M. B., Moncunill, D. F., Nechet, D., Quintana, J., Rebello, E., Rusticucci, M.,
845 Santos, J. L., Trebejo, I., Vincent, L. A., 2006. Trends in total and extreme South American rainfall in

846 1960–2000 and links with sea surface temperature. *J. Climate*, 19, 1490–1512.
847 DOI: <http://dx.doi.org/10.1175/JCLI3695.1>

848 Huang, H., Seager, R., Kushnir, Y., 2005. The 1976/77 transition in precipitation over the Americas and
849 the influence of tropical SST, *Climate Dyn.*, 24, 721–740. DOI: 10.1007/s00382-005-0015-6.

850 IPCC, 2012. Managing the risks of extreme events and disasters to advance climate change adaptation.
851 In: Field, C., Barros, V. et al (Eds.). A Special Report of Working Groups I and II of the IPCC.
852 Cambridge University Press, Cambridge, UK and New York, NY, USA (582 pp.).

853 Jacques-Coper, M., Garreaud, R. D., 2015. Characterization of the 1970s climate shift in South America,
854 *Int. J. Climatol.*, 35, 2164–2179, DOI:10.1002/joc.4120.

855 Jones, R. W., Renfrew, I. A., Orr, A. B., Webber, G. M., Holland, D. M., Lazzara, M.A., 2016. Evaluation of
856 four global reanalysis products using in situ observations in the Amundsen Sea Embayment,
857 Antarctica, *J. Geophys. Res. Atmos.*, 121, DOI:10.1002/2015JD024680.

858 Kanamitsu, M., Ebisuzaki, W., Woollen, J., Yang, S., Hnilo, J.J., Fiorino, M.M., Potter, G.L., 2002. NCEP–
859 DOE AMIP-II Reanalysis (R-2). *Bull. Amer. Meteor. Soc.*, 83,1631–1643, DOI: 10.1175/BAMS-83-11-
860 1631.

861 Kayano, M.T., Andreoli, R.V., 2007. Relation of South American summer rainfall interannual variations
862 with the Pacific decadal oscillation. *Int J Climatol.*, 27:531–540. DOI: 10.1002/joc.1417

863 Kayano, M. T., Pestrelo de Oliveira, C., Andreoli, R. V., 2009. Interannual relations between South
864 American rainfall and tropical sea surface temperature anomalies before and after 1976. *Int. J.*
865 *Climatol.* 29, 1439–1448. doi:10.1002/joc.1824

866 Klein Tank, A.M.G., Zwiers, F.W., Zhang, X., 2009. Guidelines on Analysis of Extremes in a Changing
867 Climate in Support of Informed Decisions for Adaptation, WMO-TD No. 1500/WCDMP-No. 72,
868 Geneva. 52 pp.

869 Kodama, Y. M., 1992. Large-scale common features of subtropical precipitation zones (the Baiu frontal
870 zone, the SPCZ and SACZ). 1. Characteristics of subtropical frontal zones. *J. Meteor. Soc. Japan*, 70,
871 813-836. DOI: 10.2151/jmsj1965.70.4_813

872 Krepper, C., Garcia, N., 2004. Spatial and temporal structures of trends and interannual variability of
873 precipitation over the La Plata Basin. *Q. Int.* 114, 11–21. DOI: 10.1016/S1040-6182(03)00038-7

874 Krepper, C. M., García, N. O., Jones, P. D., 2006. Paraguay river basin response to seasonal rainfall. *Int. J.*
875 *Climatol.*, 26: 1267–1278. DOI: 10.1002/joc.1313

876 Laing, A. G., Fritch, J. M., 2000. The large-scale environments of the global populations of mesoscale
877 convective complexes. *Mon. Wea. Rev.*, 128, 2756-2776. DOI: 10.1175/1520-
878 0493(2000)128<2756:TLSEOT>2.0.CO;2

879 La Nación, 2017. Inundaciones: pronostican pérdidas para el campo de hasta US\$ 1750 millones.
880 Available online at [http://www.lanacion.com.ar/1976462-inundaciones-pronostican-perdidas-](http://www.lanacion.com.ar/1976462-inundaciones-pronostican-perdidas-para-el-campo-de-hasta-us-1750-millones)
881 [para-el-campo-de-hasta-us-1750-millones](http://www.lanacion.com.ar/1976462-inundaciones-pronostican-perdidas-para-el-campo-de-hasta-us-1750-millones). Accessed February 2017.

882 Lenters, J. D., Cook, K. H., 1997. On the Origin of the Bolivian High and Related Circulation Features of
883 the South American Climate. *J. Atmos. Sci.*, 54, 656-678. DOI: 10.1175/1520-
884 0469(1997)054<0656:OTOOTB>2.0.CO;2

885 Li, F., Orsolini, Y. J., Wang, H., Gao, Y., He, S., 2018. Atlantic multidecadal oscillation modulates the
886 impacts of Arctic sea ice decline. *Geophysical Research Letters*, 45, 2497– 2506.
887 <https://doi.org/10.1002/2017GL076210>

888 Loikith, P. C., Detzer, J., Mechoso, C. R., Lee, H., Barkhordarian, A., 2017. The influence of recurrent
889 modes of climate variability on the occurrence of monthly temperature extremes over South
890 America. *Journal of Geophysical Research: Atmospheres*, 122, 297–311. DOI:
891 10.1002/2017JD027561.

892 Lovino, M. A, García, N., Baethgen, W., 2014. Spatiotemporal analysis of extreme precipitation events in
893 the Northeast region of Argentina (NEA). *J. Hydrol.: Reg. Stud.* 2, 140-158. DOI:
894 10.1016/j.ejrh.2014.09.001

895 Lovino, M. A., 2015: Environmental impact of climate variability and extreme events in the province of
896 Santa Fe (Argentina), within the climate change context. PhD thesis, Universidad Nacional del
897 Litoral, Argentina, 238 pp. <http://bibliotecavirtual.unl.edu.ar:8080/tesis/handle/11185/707>

898 Lovino, M. A., Müller, O. V., Müller, G. V., Sgroi, L. C., Baethgen, W. E., 2018. Interannual-to-
899 multidecadal Hydroclimate Variability and its Sectoral Impacts in northeastern Argentina, *Hydrol.*
900 *Earth Syst. Sci.*, 22, 3155-3174, <https://doi.org/10.5194/hess-22-3155-2018>.

901 Magrin, G. O., Travasso, M. I., Rodriguez, G. R., Solman, S. and Nuñez, M., 2009. Climate change and
902 wheat production in Argentina, *Int. J. Global Warming*, Vol. 1, Nos. 1/2/3, pp.214–226. DOI:
903 10.1504/IJGW.2009.027090

904 Magrin G.O., Travasso M.I., Mehzer R., 2012. Impacts of Climate Variability and Extremes on Crop
905 Production in Argentina. *Planet Under Pressure 2012*, INTA, Argentina. Available
906 at: [http://elsevier.conference-](http://elsevier.conference-services.net/programme.asp?conferenceID=2808&action=prog_categories)
907 [services.net/programme.asp?conferenceID=2808&action=prog_categories](http://elsevier.conference-services.net/programme.asp?conferenceID=2808&action=prog_categories). (Accessed April 18,
908 2017).

909 Magrin, G. O., J.A. Marengo, J.-P. Boulanger, M.S. Buckeridge, E. Castellanos, G. Poveda, F.R. Scarano,
910 and S. Vicuña, 2014: Central and South America. In: *Climate Change 2014: Impacts, Adaptation,*
911 *and Vulnerability. Part B: Regional Aspects. Contribution of Working Group II to the Fifth*
912 *Assessment Report of the Intergovernmental Panel on Climate Change* [Barros, V.R., C.B. Field, D.J.
913 Dokken, M.D. Mastrandrea, K.J. Mach, T.E. Bilir, M. Chatterjee, K.L. Ebi, Y.O. Estrada, R.C. Genova,
914 B. Girma, E.S. Kissel, A.N. Levy, S. MacCracken, P.R. Mastrandrea, and L.L. White (eds.)]. Cambridge
915 University Press, Cambridge, United Kingdom and New York, NY, USA, pp. 1499-1566.

916 Marengo, J.A., 2004. Interdecadal variability and trends of rainfall across the Amazon basin. *Theor.*
917 *Appl. Climatol.* 78, 79–96. DOI: 10.1007/s00704-004-0045-8

918 Marengo, J. A., Liebmann, B., Grimm, A. M., Misra, V., Silva Dias, P. L., Cavalcanti, I. F. A., Carvalho, L. M.
919 V., Berbery, E. H., Ambrizzi, T., Vera, C. S., Saulo, A. C., Nogues-Paegle, J., Zipser, E., Seth, A., Alves,
920 L. M., 2012. Recent developments on the South American monsoon system. *Int. J. Climatol.*, 32: 1–
921 21. doi:10.1002/joc.2254

922 Mayer, L. I, Rattalino Edreira, J. I., Navarrete Sánchez, R.A, Maddonni, G.A., Otegui, M.E, 2012. Effect of
923 high temperatures on maize productivity (In Spanish). XX Congreso Aapresid "20 veces sí"
924 [http://www.string-agro.com/aapresid/archivo/2012/ponencias/C20_010.pdf] accessed April
925 2017.

926 Mo, K. C, Berbery, E. H., 2011. Drought and Persistent Wet Spells over South America Based on
927 Observations and the U.S. CLIVAR Drought Experiments, *J. Climate*, 24, 1801–1820, doi:
928 10.1175/2010JCLI3874.1.

929 Moron, V., Vautard, R., Ghil, M., 1998. Trends, interdecadal and interannual oscillations in global sea-
930 surface temperatures *Climate Dynamics*, 14: 545-569. DOI: 10.1007/s003820050241

931 Müller, G., Nuñez, M. Seluchi, M., 2000: Relationship between ENSO cycles and frost events within the
932 Pampa Húmeda region. *Int. J. Climatol.*, 20, 1619–1637. DOI: 10.1002/1097-
933 0088(20001115)20:13<1619::AID-JOC552>3.0.CO;2-F.

934 Müller, G. V, Compagnucci, R., Nuñez, M., Salles, A., 2003. Surface Circulation Associated with Frosts in
935 the Wet Pampas. *International Journal of Climatology*, 23, 8, 943-961. DOI: 10.1002/joc.907.

936 Müller, O. V., Berbery, E. H., Alcaraz-Segura, D., Ek, M. B., 2014. Regional Model Simulations of the 2008
937 Drought in Southern South America Using a Consistent Set of Land Surface Properties. *J.*
938 *Climate*, 27, 6754–6778, DOI: 10.1175/JCLI-D-13-00463.1.

939 National Geographic Institute (NGI), 2015: Geographical Atlas of the Argentine Republic (In Spanish).
940 Distal Editorial, Buenos Aires, Argentina, 330 pp. ISBN 9789874571908.

941 Nogués-Paegle, J., Mechoso, C., Fu, R., Berbery, E. H., Winston, C., Chen, T-C., Cook, K., Diaz, A., Enfield,
942 D., Ferreira, R., Grimm, A., Kousky, V., Liebmann, B., Marengo, J., Mo., K., Neelin, L., Paegle, J.,
943 Robertson, A., Seth, A., Vera, C., Zhou, J., 2002. Progress in Pan American CLIVAR Research:
944 Understanding the South American Monsoon. *Meteorológica*, 27, 3-32.

945 Okabe, A., Boots, K. Sugihara, 2000. Spatial Tessellations Concepts and Applications of Voronoi
946 Diagrams, Second Edition. John Wiley, New York, United States.

947 Rasmussen, K. L., M.M. Chaplin, M.D. Zuluaga, Houze, R.A., 2016. Contribution of Extreme Convective
948 Storms to Rainfall in South America. *J. Hydrometeor.*, 17,353–367, DOI: 10.1175/JHM-D-15-
949 0067.1.

950 Rondanini, D., Mantese, A., Savín R., Hall, A. J., 2006. Responses of sunflower yield and grain quality to
951 alternating day/night high temperature regimes during grain filling: Effects of timing, duration and
952 intensity of exposure to stress. *Field Crop Research* 96: 48-62. DOI: 10.1016/j.fcr.2005.05.006.

953 Rusticucci, M.M., Kousky, V.E., 2002. A comparative study of maximum and minimum temperatures
954 over Argentina: NCEP-NCAR reanalysis versus station data. *J Clim* 15: 2089–2101. DOI:
955 10.1175/1520-0442(2002)015<2089:ACSOMA>2.0.CO;2

956 Rusticucci, M., 2012. Observed and simulated variability of extreme temperature events over South
957 America. *Atmospheric Research*, 106, 1–17. DOI: 10.1016/j.atmosres.2011.11.001

958 Rusticucci, M., Kyselý, J., Almeida, G., Lhotka, O., 2015: Long-term variability of heat waves in Argentina
959 and recurrence probability of the severe 2008 heat wave in Buenos Aires. *Theor Appl Climatol.*,
960 DOI: 10.1007/s00704-015-1445-7.

961 Rusticucci, M., Barrucand, M. and Collazo, S., 2016. Temperature extremes in the Argentina central
962 region and their monthly relationship with the mean circulation and ENSO phases. *Int. J. Climatol.*
963 DOI: 10.1002/joc.4895

964 Schmidt, K.M., Swart, S., Reason, C. Nicholson, N., 2017. Evaluation of Satellite and Reanalysis Wind
965 Products with In Situ Wave Glider Wind Observations in the Southern Ocean. *J. Atmos. Oceanic*
966 *Technol.*, 34, 2551–2568, <https://doi.org/10.1175/JTECH-D-17-0079.1>

967 Seager, R., Naik, N., Baethgen, W., Robertson, A., Kushnir, Y., Nakamura, J., Jurburg, S., 2010. Tropical
968 Oceanic Causes of Interannual to Multidecadal Precipitation Variability in Southeast South America
969 over the Past Century. *J. Climate*, 23, 5517–5539. DOI: 10.1175/2010JCLI3578.1

970 Sen, P.K., 1968. Estimates of the regression coefficient based on Kendall's tau. *Journal of the American*
971 *Statistical Association* 63, 1379–1389.

972 Seneviratne, S.I., Nicholls, D. Easterling, C.M. Goodess, S. Kanae, J. Kossin, Y. Luo, J. Marengo, K.
973 McInnes, M. Rahimi, M. Reichstein, A. Sorteberg, C. Vera, and X. Zhang, 2012: Changes in climate
974 extremes and their impacts on the natural physical environment. In Field, C.B., V. Barros, T.F.
975 Stocker, D. Qin, D.J. Dokken, K.L. Ebi, M.D. Mastrandrea, K.J. Mach, G.-K. Plattner, S.K. Allen, M.
976 Tignor, and P.M. Midgley (eds.), *Managing the Risks of Extreme Events and Disasters to Advance*
977 *Climate Change Adaptation. A Special Report of Working Groups I and II of the Intergovernmental*
978 *Panel on Climate Change (IPCC)*. Cambridge University Press, Cambridge, UK, and New York, NY,
979 USA, pp. 109-230.

980 Sillmann, J., Kharin, V. V., Zhang, X., Zwiers, F. W., Bronaugh, D., 2013. Climate extremes indices in the
981 CMIP5 multimodel ensemble: Part 1. Model evaluation in the present climate, *J. Geophys. Res.*
982 *Atmos.*, 118, 1716–1733. doi:10.1002/jgrd.50203

983 Silva, V.B., Kousky, V.E. , Higgins, R.W., 2011. Daily Precipitation Statistics for South America: An
984 Intercomparison between NCEP Reanalyses and Observations. *J. Hydrometeor.*, 12, 101–117, doi:
985 10.1175/2010JHM1303.1

986 Skansi, M. M., Brunet, M., Sigró, J., Aguilar, E., Arevalo Groening, J. A., Betancour, O. J., Castellón Geier,
987 Y. R., Correa Amaya, R. L., Jácome, H., Malherios Ramos, A., Oria Rojas, C., Pasten, A., Sallons Mitro,
988 S., Villaroel, C., Martínez, R., Alexander, L. V., Jones, P. D., 2013. Warming and wetting signals
989 emerging from analysis of changes in climate extreme indices over South America. *Global and*
990 *Planetary Change* 100, 295–307. DOI: 10.1016/j.gloplacha.2012.11.004.

991 Stocker, T.F., D. Qin, G.-K. Plattner, L.V. Alexander, S.K. Allen, N.L. Bindoff, F.-M. Bréon, J.A. Church, U.
992 Cubasch, S. Emori, P. Forster, P. Friedlingstein, N. Gillett, J.M. Gregory, D.L. Hartmann, E. Jansen, B.
993 Kirtman, R. Knutti, K. Krishna Kumar, P. Lemke, J. Marotzke, V. Masson-Delmotte, G.A. Meehl, I.I.
994 Mokhov, S. Piao, V. Ramaswamy, D. Randall, M. Rhein, M. Rojas, C. Sabine, D. Shindell, L.D. Talley,
995 D.G. Vaughan and S.-P. Xie, 2013: Technical Summary. In: *Climate Change 2013: The Physical*
996 *Science Basis. Contribution of Working Group I to the Fifth Assessment Report of the*
997 *Intergovernmental Panel on Climate Change* [Stocker, T.F., D. Qin, G.-K. Plattner, M. Tignor, S.K.
998 Allen, J. Boschung, A. Nauels, Y. Xia, V. Bex and P.M. Midgley (eds.)]. Cambridge University Press,
999 Cambridge, United Kingdom and New York, NY, USA.

1000 Vautard R., 1995. Patterns in time: SSA and MSSA. In Chapter 14 of *Analysis of Climate Variability:*
1001 *applications of Statistical Techniques*, von Storch H, Navarra A (eds). Springer Verlag: Berlin, 327.

1002 Vera, C., Vigliarolo, P. K., Berbery, E.H., 2002. Cold season synoptic scale waves over subtropical South
1003 America. *Mon. Wea. Rev.*, 130, 684–699. DOI: 10.1175/1520-
1004 0493(2002)130<0684:CSSSWO>2.0.CO;2

1005 Verón, S. R., de Abelleira, D., Lobell, D., 2015. Impacts of precipitation and temperature on crop yields
1006 in the Pampas. *Climatic Change*, 130, 235–245, DOI:10.1007/s10584-015-1350-1.

1007 Wang, X. L., Swail, V. R, 2001. Changes of extreme wave heights in Northern Hemisphere oceans and
1008 related atmospheric circulation regimes. *J. Clim.*, 14, 2204–2220. DOI: 10.1175/1520-
1009 0442(2001)014<2204:COEWHI>2.0.CO;2

1010 Wang, X. L., H. Chen, Y. Wu, Y. Feng, and Q. Pu, 2010: New techniques for detection and adjustment of
1011 shifts in daily precipitation data series. *J. Appl. Meteor. Climatol.* 49 (No. 12), 2416-2436. DOI:
1012 10.1175/2010JAMC2376.1

1013 Wang, A., Zeng, X., 2012. Evaluation of multireanalysis products with in situ observations over the
1014 Tibetan Plateau, *J. Geophys. Res.*, 117, D05102, DOI: 10.1029/2011JD016553.

1015 Winchester, L., Szalachman, R., 2009. The Urban Poor's Vulnerability to the Impacts of Climate Change
1016 in Latin America and the Caribbean. A Policy Agenda. Presented at the 5th Urban Research
1017 Symposium "Cities and Climate Change: Responding to the Urgent Agenda" June 28-30, 2009,
1018 Marseille, France, The World Bank, Washington, DC, USA, 31 pp.
1019 [http://siteresources.worldbank.org/INTURBANDEVELOPMENT/Resources/336387-](http://siteresources.worldbank.org/INTURBANDEVELOPMENT/Resources/336387-1342044185050/8756911-1342044630817/V2Chap28.pdf)
1020 [1342044185050/8756911-1342044630817/V2Chap28.pdf](http://siteresources.worldbank.org/INTURBANDEVELOPMENT/Resources/336387-1342044185050/8756911-1342044630817/V2Chap28.pdf)

1021 Wilks D. S., 2006: *Statistical Methods in the Atmospheric Sciences*, Elsevier Inc, UK. 627 pp.

1022 Wolter, K., and M. S. Timlin, 2011: El Niño/Southern Oscillation behaviour since 1871 as diagnosed in an
1023 extended multivariate ENSO index (MEI.ext). *Intl. J. Climatology*, 31, 1074-1087. DOI:
1024 10.1002/joc.2336

1025 Yang, E. Kim, H.M., 2017. Evaluation of a Regional Reanalysis and ERA-Interim over East Asia Using In
1026 Situ Observations during 2013–14. *J. Appl. Meteor. Climatol.*, 56, 2821–2844. DOI: 10.1175/JAMC-
1027 D-16-0227.1

1028 Young, K. C., 1992. A three-way model for interpolating monthly precipitation values. *Mon. Wea. Rev.*,
1029 120, 2561–2569. DOI: 10.1175/1520-0493(1992)120<2561:ATWMFI>2.0.CO;2

1030 Zaninelli P., Carril A. F., Menéndez C. G., 2015. Exploring maximum and minimum temperatures in
1031 different reanalysis. Part 1: Means season patterns (In Spanish). *Meteorologica* 40: 43–58

1032 Zhang, X., Vincent, L.A., Hogg, W.D., Niitsoo, A., 2000. Temperature and precipitation trends in Canada
1033 during the 20th century. *Atmosphere-Ocean* 38, 395–429. DOI: 10.1080/07055900.2000.9649654

- 1034 Zhang, X., Hegerl, G., Zwiers, F.W. Kenyon, J., 2005. Avoiding inhomogeneity in percentile-based indices
1035 of temperature extremes. *J. Climate*, 18, 1641-1651. DOI: 10.1175/JCLI3366.1
- 1036 Zhang, X., Alexander, L.V., Hegerl, G.C., Klein-Tank, A., Peterson, T.C., Trewin, B., Zwiers, F.W., 2011.
1037 Indices for monitoring changes in extremes based on daily temperature and precipitation data.
1038 *Wiley Interdisciplinary Reviews: Climate Change* 2, 851–870 DOI: 10.1002/wcc.147.
- 1039 Zhou, J., Lau, K., 1998. Does a Monsoon Climate Exist over South America?. *J. Climate*, 11, 1020–1040.
1040 [https://doi.org/10.1175/1520-0442\(1998\)011<1020:DAMCEO>2.0.CO;2](https://doi.org/10.1175/1520-0442(1998)011<1020:DAMCEO>2.0.CO;2)
- 1041 Zipser, E. J., D. J. Cecil, C. Liu, S. W. Nesbitt, and D. P. Yorty, 2006: Where are the most intense
1042 thunderstorms on Earth? *Bull. Amer. Meteor. Soc.*, 87, 1057–1071, DOI: 10.1175/ BAMS-87-8-
1043 1057.